Saturated Proteostasis and Nuclear Injuries Defeat Homeostatic Potentials of α-Synuclein Filaments

Shemin Mansuri, Richa Singh, Shivali Rawat, Aanchal, Debodyuti Mondal and Swasti Raychaudhuri [#]

CSIR-Centre for Cellular and Molecular Biology, Uppal Road, Hyderabad - 500007, India

[#] Correspondence to: rcswasti@ccmb.res.in

Highlights

- α-Synuclein accumulates into two distinct inclusion bodies for subsequent quality control – cytoskeleton-driven aggresomes and seeding-based filamentous inclusions
- Repurposing of proteostasis-factors into overgrown filamentous inclusions saturates protein homeostasis
- Growing perinuclear filamentous inclusions compromises nuclear integrity by exerting dynein-mediated mechanical stress on nuclear lamina
- Opportunistic degradation of filamentous inclusions restores cellular equilibrium

Keywords:

α-Synuclein, inclusion bodies, Syn-aggresomes, Syn-filaments, proteostasis over-saturation, Nuclear envelope injury

Abstract

Biogenesis of inclusion bodies (IBs) contributes to protein quality control (PQC). Perinuclear IBs like aggresomes/JUNQs serve as sites for ubiquitin-proteasome mediated protein degradation. The other canonical IB, IPOD, does not degrade but sequesters non-ubiquitinated terminally aggregated proteins to prevent their promiscuous interactions and interferences with other cellular functions. Here, we show that as a deviation from this convention, misfolding-prone α-Synuclein is simultaneously deposited into two distinct IBs – Syn-aggresomes and seeding based filamentous inclusions (Syn-filaments), both acting as sites for ubiquitin-proteasome mediated protein degradation. Syn-aggresomes buffer the spontaneous turnover of α-Synuclein. Syn-filaments serve the dual purpose of self-sequestration and opportunistic degradation. Counterintuitively, overgrowth of perinuclear Syn-filaments titrates out cellular PQC-pool and challenges the turnover and solubility of other misfolding-prone proteins. Moreover, large Syn-filaments associate with LaminB1, mount mechanical stress on nuclear envelope via dynein, disrupt nuclear integrity, and deregulate stress-triggered transcription of chaperones failing their homeostatic potential.

Introduction

Over the past decades, 'Sequestration' into inclusion bodies (IBs) has been identified as a potent strategy to facilitate quality control (QC) of misfolding-prone proteins (Chen, Retzlaff et al., 2011, Sontag, Vonk et al., 2014)). The current consensus suggests broadly three kinds of IBs. Readily reversible amorphous blobs of misfolded proteins scattered in stressed cells are called stress foci (Song, Yang et al., 2014, Spokoini, Moldavski et al., 2012). The second type represents the perinuclear IBs where misfolded and ubiquitinated proteins are sequestered for localized proteasome-mediated degradation. These are termed as aggresomes or juxtanuclear quality control compartments (JUNQs) based on their cytoskeleton-based biogenesis (Johnston, Ward et al., 1998, Kaganovich, Kopito et al., 2008, Tyedmers, Mogk et al., 2010a). The third type that quarantines the excess misfolded proteins upon saturation of aggresomes and JUNQs are known as insoluble protein deposits (IPODs). IPODs may be peripheral or perinuclear depending on their cytoskeleton association and are inefficiently processed by the ubiquitin-proteasome system (UPS) (Kaganovich et al., 2008, Kumar, Nawroth et al., 2016, Weisberg, Lyakhovetsky et al., 2012). Rather, IPODs are positive for autophagosome cargo markers and may also be diluted through retention in one of the daughter cells during mitotic division (Ogrodnik, Salmonowicz et al., 2014).

Many amyloidogenic proteins including mutant Huntingtin, Rnq1, Ure2, and Sup35 directly accumulate into IPODs due to their intrinsic property of self-assembly and inefficient ubiquitination (Chen et al., 2011, Kaganovich et al., 2008, Tyedmers, Treusch et al., 2010b). Soluble and oligomeric forms of these amyloid proteins interact with many cellular proteins (Buratti & Baralle, 2012, Kim, Hosp et al., 2016, McFarland, Ellis et al., 2008, Olzscha, Schermann et al., 2011). Faster sequestration into IPOD-like inclusions reduce their promiscuous interactions and limit interferences with vital cellular processes (Treusch, Cyr et al., 2009, Weisberg et al., 2012). Amyloidogenic proteins also occasionally accumulate into

perinuclear UPS-degradable IBs in mammalian cells, possibly as an intermediate state of IPOD-biogenesis (Taylor, Tanaka et al., 2003), but may cause toxicity by delaying degradation of other misfolding prone proteins (Waelter, Boeddrich et al., 2001).

α-Synuclein is also an amyloidogenic protein. Unlike the compact immobile deposits that are observed for Huntingtin and other IPOD-forming amyloids (Bauerlein, Fernandez-Busnadiego et al., 2020), α-Synuclein accumulate into comparatively loosely-packed filamentous IBs known as Lewy Bodies (LB) at the perinucleus of the neurons of Synucleopathy patients and mouse models (Curran & Wrigley, 1997, Galloway, Mulvihill et al., 1992). Amyloid filaments of α-Synuclein radiate at the periphery of LBs and are also observed as independent filaments distant to the LBs known as Lewy Body filaments (LFs) or Lewy neurites (LNs) (Forno, 1996, Lashuel, 2020, Spillantini, Crowther et al., 1998). Mature LBs are marked with ubiquitinated proteins at the core and contain multiple PQC-factors but are never found to be disintegrated or degraded in mouse models or in patients' brains. Therefore, LBs are considered as 'failed aggresomes'(McNaught, Shashidharan et al., 2002, Olanow, Perl et al., 2004); although their protein turnover potential and other homeostatic advantages or disadvantages could never be investigated extensively due to lack of convenient experimental models.

Only recently, addition of recombinant α-Synuclein fibrils as seeds has been shown to recapitulate the biogenesis of LB-like IBs of endogenous α-Synuclein in primary neurons (Luk, Song et al., 2009, Volpicelli-Daley, Luk et al., 2011). In terms of template-based biogenesis and filamentous morphology, these IBs are distinct from the aggresome-like α-Synuclein blobs that are observed in cell culture by its over-expression (Engelender, Kaminsky et al., 1999, Lazaro, Rodrigues et al., 2014, Nonaka & Hasegawa, 2009), by liquid-liquid phase separation (LLPS) (Ray, Singh et al., 2020), or upon cellular homeostasis deregulation (Lee, Shin et al., 2002, McLean, Kawamata et al., 2001). Here, we report that α-

Synuclein can be simultaneously deposited into cytoskeleton driven aggresome-like IBs (Syn-aggresomes) and seeding-based LB-like filamentous IBs (Syn-filaments) in mitotic cells. Biogenesis of perinuclear Syn-aggresomes represents a spontaneous response of the cellular-PQC to sequester and degrade misfolding-prone α-Synuclein. On the other hand, perinuclear Syn-filaments are recognized by the cellular PQC at a later stage of IB-biogenesis and serve as sites for UPS-mediated opportunistic degradation. This suggests that sequestration into terminally aggregated IPODs is not the universal homeostatic strategy to sequester all amyloid proteins. Further, we show that while Syn-aggresomes consistently facilitate cellular homeostasis, polymerization into over-grown Syn-filaments accompanies inadvertent homeostatic costs. Large Syn-filaments increasingly attract PQC-factors to oversaturate proteostasis, collaborate with cytoskeleton to associate with the nuclear lamina and stretch and distort the nuclear envelope. Existence of Syn-aggresomes and Syn-filaments, nuclear-encaging by Syn-filaments and nuclear injuries are also observed in primary neurons. We propose that, despite having homeostatic potentials, sequestration of α-Synuclein into Syn-filaments may contribute to toxicity in post-mitotic neurons at the chronic proteostasis-stress setting of age-related Synucleopathies.

Results

A cell culture model recapitulating filamentous inclusions of α-Synuclein

We prepared multiple stable and inducible lines in Hek293T and Neuro2a cells over-expressing α-Synuclein variants tagged with EGFP at the C-terminus (SNCA-EGFP). Wild type SNCA-EGFP was diffusely distributed throughout the cell including the nucleus (**Fig. 1A and S1A**). Filamentous inclusions of wild type SNCA-EGFP was not observed even upon prolonged seeding with 1 μM recombinant α-Synuclein fibrils (preformed fibrils, PFF) (**Fig. 1A**). *In vitro* fibrilization propensity of α-Synuclein with Parkinson's Disease familial

mutations A30P and A53T differ from the wild type (Conway, Lee et al., 2000a, Conway, Lee et al., 2000b). We observed that the formation of fibrils was slower for A30P and faster for A53T than the wild type SNCA in Thioflavin T assay (**Fig. S1B**). The (A30P + A53T) double mutant (SNCA(DM)), which recapitulates the early onset degenerative phenotypes of Synucleopathies in mouse models (Kilpelainen, Julku et al., 2019, Richfield, Thiruchelvam et al., 2002), showed a lag-time between wild type and A30P (**Fig. S1B**). Far-UV circular dichroism (CD) spectra confirmed identical intrinsic disorder in monomers and similar β-sheet content in fibrils of the wild type and each of the α-Synuclein variants (**Fig. S1C)**. Similar fibrillar structure of all the variants was seen by transmission electron microscopy (**Fig. S1D**).

Similar to wild type, C-terminal EGFP-tagged versions of other α-Synuclein variants were present throughout the cells upon over-expression in Hek293T (**Fig. 1A**). Among these, only A53T and DM over-expressing cells showed filamentous inclusion bodies (filamentous IBs; Syn-filaments) after prolonged seeding (**Fig. 1A**, arrowheads). Number of Syn-filament containing cells was more in case of SNCA(DM) than SNCA(A53T) (**Fig. 1B**). We observed multiple initiation sites of filament biogenesis that converged into large skein-like filaments (**Fig. 1C, S1E and supplementary video 1**). Small Syn-filaments first appeared in the cytoplasm after 3 days of seeding followed by formation of bundle of filaments. These bundle of filaments gradually merged into skein-like filamentous IBs encaging the nucleus. The 6th day cell population was heterogeneous showcasing different stages of filament biogenesis. Large skein-like IBs were mostly perinuclear and observed in more than 60 % of the filament-containing cells (**Fig. 1D**). Skein-like deposits were also observed inside the nucleus or distant to the nucleus (**Fig. S1Fii-iii**, arrowheads).

Syn-filaments were also observed in Neuro2a cells at day 6 after seeding (**Fig. S1G**). Filament formation did not depend on the EGFP tag as both untagged and mCherry-tagged

SNCA(DM) cells displayed Syn-filaments (**Fig. S1H**). The recombinant Syn-fibrils entered cells within 1 hr of incubation and were required for Syn-filament formation in a dose dependent manner (**Fig. S1I**). Filament formation was prevented by Congo Red (CR) **(Fig. S1J)**, a beta sheet fold binding dye known to prevent *in vitro* fibrilization of α-Synuclein and other amyloids by inhibiting oligomerization (Lendel, Bertoncini et al., 2009, Sanchez, Mahlke et al., 2003).

Canonical Lewy bodies (LBs) are marked by the presence of phosphorylated α-Synuclein and various PQC components. Mature LBs also engulf membranous organelles (Curran & Wrigley, 1997, Mahul-Mellier, Burtscher et al., 2020). Syn-filaments were always stained by phospho-Ser129-Synuclein (p129-Syn) antibody in our cells. Ubiquitin, autophagosome cargo marker Sequestosome 1 (SQSTM-1/p62) and LC3 antibodies stained the large filamentous IBs at the core but the peripheral and smaller filaments remained unrecognized (**Fig. 1E**). Further, bigger perinuclear Syn-filaments partially co-localized with organelles like mitochondria, endoplasmic reticulum (ER) and lysosome, and partly distorted their morphology and cellular distribution (**Fig. 1F,** arrowheads). Thus, the Syn-filaments observed in our cell culture model resembled LBs at various stages of biogenesis.

Syn-filaments serve as Opportunistic Quality Control Sites for α-Synuclein

In addition to the filamentous inclusions, we observed an additional blob-like perinuclear deposit of SNCA(DM)-EGFP that was also positive for p129-Syn antibody (**Fig. 2A, S1A and S2A,** arrowheads). These deposits were single copy per cell and independent entities very close or far to the Syn-filaments. Distinct blobs of SNCA(DM)-EGFP were not apparent in acetone-methanol fixed cells but globular perinuclear blobs stained with p129-Syn antibody were noticed (**Fig. 1Ei,** arrowhead). p129-Syn positive perinuclear blobs were observed even in unseeded cells within 24 hrs of overexpression (**Fig. 2A and S2A**). Since

we observed two independent IBs of α-Synuclein in same cells, we investigated their homeostatic contributions and compared them with the canonical QC deposits.

Aggresomes are active sites for degradation of misfolding-prone proteins positioned at the microtubule organizing centre (MTOC) and co-stained with γ-tubulin (Johnston et al., 1998). Two distinct perinuclear dots of γ-tubulin were observed in SNCA(DM)-EGFP uninduced cells (**Fig. 2B,** arrowhead). These γ-tubulin dots were merged into blobs upon induction of SNCA(DM)-EGFP and were also encircled by SQSTM1 (**Fig. 2B and S2B,** arrowheads). Similar γ-tubulin blobs were observed both close and far to the Syn-filaments in PFF treated cells but Syn-filaments were never positioned on γ-tubulin (**Fig. 2B and S2B**). SQSTM1 also encased the perinuclear SNCA(DM)-EGFP blobs irrespective of the existence of Syn-filaments (**Fig. 2C and S2C,** arrowheads). Aggresome/JUNQ-like QC-deposits are typically composed of ubiquitinated proteins (Kaganovich et al., 2008). Perinuclear blobs stained by ubiquitin antibody were prominent in SNCA(DM)-EGFP overexpressing cells in presence and absence of PFF and Syn-filaments (**Fig. 2D and S2D,** arrowheads).

As mentioned above, p129-Syn antibody positive blobs served as perinuclear accumulation sites for SNCA(DM)-EGFP even in unseeded cells (**Fig. 2A**). p129-Syn was more degradation-prone than the non-phosphorylated counterpart (**Fig. 2E**). Protein load of p129-Syn was increased after proteasome inhibitor MG132 treatment (**Fig. 2F)**. Simultaneously, size of the p129-Syn blobs were comparatively reduced and p129-Syn was dispersed throughout the cells (**Fig. 2F and S2E**, arrowheads). This data suggested a connection of ubiquitin-proteasome machinery with these perinuclear sites. Further, encircling of SNCA(DM)-EGFP blobs by SQSTM1 (**Fig. 2C**) indicated involvement of autophagy pathway. Microtubules contribute to the biogenesis of canonical aggresomes/JUNQs (Johnston et al., 1998). SNCA(DM)-EGFP blobs disappeared within 30 min of nocodazole treatment (**Fig. 2G**, arrowhead), a small molecule that disrupts

microtubule assembly. Simultaneously, cycloheximide chase assay revealed degradation of p129-Syn was delayed in nocodazole-treated cells (**Fig. 2G**). Thus, the SNCA(DM)-EGFP blobs resembled aggresome-like PQC-IBs serving a spontaneous cellular response to sequester degradable α-Synuclein. Hereafter, we call these blobs as Syn-aggresomes. In presence of Syn-aggresomes, both α-Synuclein and p129-Syn level never increased in unseeded cells even after 6 days of continuous overexpression (**Fig. 2H**).

Interestingly, total α-Synuclein load did not increase in PFF-treated 6th day SNCA(DM)-EGFP cells also although p129-Syn level was higher (**Fig. 2H**). Lysing the cells with 1% Triton-X 100 yielded soluble and insoluble fractions (**Fig. S2F**). α-Synuclein or p129-Syn load remained unchanged in the soluble fraction but were increased in the insoluble fraction (**Fig. 2H**). Intriguingly, the increase of α-Synuclein in the insoluble fraction was not justifiably proportionate the large Syn-filaments observed in microscopy indicating 'biochemical softness' of the filamentous IBs. These blots further suggested that while a fraction of α-Synuclein was being degraded *via* aggresome, another fraction was increasingly phosphorylated, polymerized into Syn-filaments in presence of PFF, and turned sparingly insoluble. Remarkably, increase in p129-Syn level in total and insoluble fraction of 6th day PFF-treated SNCA(DM)-EGFP cells was prevented in presence of Congo Red that compromised polymerization efficiency of Syn-filaments (**Fig. S2G**).

Next, we trypsinized and re-plated the 6th day Syn-filament containing cells. When we withdrew PFF-seeds or stopped synthesis of new SNCA(DM)-EGFP by removing doxycycline during re-plating, the filamentous IBs first disintegrated into multiple smaller scattered cytoplasmic blobs and then disappeared (**Fig. 2I-J**). Simultaneously, α-Synuclein and p129-Syn levels reduced significantly confirming degradation of the protein (**Fig. 2K)**. When the replating was done in presence of MG132, p129-Syn bands remained stabilized suggesting contribution of ubiquitin-proteasome system (UPS) in the degradation process

(**Fig. 2L**). Treating the 6th day Syn-filament containing cells with Congo Red during replating resulted in reduction of p129-Syn even in presence of PFF (**Fig. 2M**). Altogether, Syn-filaments were UPS-degradable if their polymerization was impeded and therefore represented opportunistic degradation sites for α-Synuclein.

Cellular homeostasis is near saturation in Syn-filament containing cells

Does the biogenesis of Syn-aggresomes or Syn-filaments impair cellular homeostasis like many other amyloid deposits? Syn-aggresome containing cells proliferated efficiently. As per MTT assay, cell viability also remained unperturbed despite the presence of Syn-filaments in ~ 40% of the 6th day PFF-treated SNCA(DM)-EGFP cells (**Fig. 1B and 3A**). Further, Syn-filaments were asymmetrically partitioned into the daughter cells without compromising mitotic division (**Fig. 3Bi, S3A and supplementary video 2**). Infrequently, nuclear entry of large skein-like filaments was observed in live cell microscopy fragmenting the nuclei and cell detachment from the plate surface (**Fig. 3C, S3B and supplementary video 3**).

According to the proteostasis theory of protein aggregation diseases, aggregating amyloids trap and sequester many essential cellular proteins during deposition into IBs and thereby deregulate vital cellular processes (Culver, Savas et al., 2012, Olzscha et al., 2011). It is also proposed that IPOD-like IBs seclude aggregation prone amyloidogenic proteins from the rest of the proteome, reduce non-specific interactions and protect cellular function (Ramdzan, Trubetskov et al., 2017, Tyedmers et al., 2010a). SILAC-based quantitative mass spectrometry of the total, soluble and insoluble fractions revealed almost unperturbed proteome-balance in 6th day PFF-treated SNCA(DM)-EGFP cells (**Fig. 3D and S3C, Table S1-S3**). Large skein-like Syn-filaments observed in our study partially co-localized with mitochondria and ER (**Fig. 1F**). Moreover, Syn-filaments were perinuclear and sometimes

triggered nuclear fragmentation (**Fig. 3C**). Mitochondrial proteins were non-significantly increased in all the proteome fractions suggesting a possible adjustment in mitochondrial biology (**Fig. 3D, Table-S1**). Nuclear proteins were slightly increased in soluble fraction while decreased in insoluble fraction (**Fig. 3D**).

Despite the recruitment of multiple PQC factors into both Syn-aggresomes (**Fig. 2D-F**) and large Syn-filaments (**Fig. 1E**), chaperones and degradation machinery components were not increased in 6th day PFF treated SNCA(DM)-EGFP cells (**Fig. 3E, Table-S2**). This contradiction suggested that the association between PQC-factors and Syn-filaments was only transient. To test whether this transient repurposing was sufficient to trigger shortage of PQC-factors for other metastable proteins, we overexpressed misfolding-prone FlucDM-mCherry (Gupta, Sharif et al.) in 6th day SNCA(DM)-EGFP cells. It was deposited into the Syn-aggresomes in absence of PFF suggesting that the spontaneous cellular response of directing metastable proteins into the perinuclear QC-sites remained active (**Fig. 3Fi,** arrowhead). Excess FlucDM-mCherry did not accumulate in these cells suggesting that co-presence of α-Synuclein did not compromise aggresome-assisted turnover of this marginally stable protein (**Fig. 3G**).

Remarkably, in addition to partial co-localization with both Syn-aggresomes and large Syn-filaments (**Fig. 3Fii**, white arrowheads), FlucDM-mCherry appeared in additional cytoplasmic IBs in several Syn-filament containing cells (**Fig. 3Fiii**, blue arrowheads). Protein-load of FlucDM-mCherry was also increased in total and insoluble fractions of 6th day PFF treated SNCA(DM)-EGFP cells (**Fig. 3G**). These results suggested that the mechanism of depositing misfolding-prone proteins into canonical QC-deposits was either saturated or defective in presence of Syn-filaments compromising their turnover. Intriguingly, separate IBs of FlucDM-mCherry were absent in cells with small Syn-filaments indicating that over-saturation of cellular-PQC was manifested only after maturation of large

perinuclear Syn-filaments but not during the course of their biogenesis (**Fig. 3Fii**). To investigate further, we applied widespread proteome misfolding stress by incubating the 6th day PFF treated SNCA(DM)-EGFP cells at 42°C for 2 hr. Viability of these cells was significantly reduced after the treatment (**Fig. 3H**). Transcription upregulation of stress chaperone Hsp70 was also deregulated in the heat stressed PFF-treated SNCA(DM)-EGFP cells substantiating their susceptibility to protein-misfolding stresses (**Fig. 3I**).

Syn-filaments trigger nuclear envelope deformities

Transcription is a nucleus mediated cellular function and was deregulated in Syn-filament containing cells (**Fig. 3I**). Occasional intra-nuclear localization of Syn-filaments and nuclear fragmentation was also observed in live cell microscopy (**Fig. 3C)**. These prompted us to investigate the nuclear shape, size and integrity in detail. Staining with nuclear envelope (NE) protein Lamin B1 (LmnB1) revealed prominent increase in nuclear lamina discontinuity in Syn-filament-containing cells (**Fig. 4A-B**, arrowheads). LmnB1 was often found to be partially co-localized with Syn-filaments and lamina disintegrity was observed both near and far to the perinuclear filaments (**Fig. 4Bii-iii)**. Co-staining with LmnB1 was observed at the core of the large skein-like deposits (**Fig. 4Bi-ii**) and also at the outer periphery of the large perinuclear Syn-filaments (**Fig. 4Biv**). Large gaps in lamina were observed in these cells suggesting that Syn-filaments were penetrating into nucleus by stretching the lamina barrier (**Fig. 4Biv**). Occasionally, skein-like Syn-IBs were co-stained with LmnB1 antibody despite being far from the unperturbed nuclear lamina (**Fig. 4Bi**). In contrast, smaller Syn-filaments, both perinuclear and non-perinuclear, were mostly unstained by LmnB1 (**Fig. S4A**).

We categorized the nuclear deformities in Syn-filament containing cells depending on DAPI and LmnB1 staining (**Fig. 4C-D**, arrowheads). Kidney-shaped nuclei were observed in ~ 15-20 % of the cells where skein-like filaments were confined within NE-invaginations

(**Fig. 4Di**). As seen in laminopathies (De Vos, Houben et al., 2011, Hatch, 2018, Hatch & Hetzer, 2016), nuclear hernia-like blobs were captured in live cell microscopy (**Fig. S4B and Supplementary video 4**). Extranuclear DAPI blobs confined within LmnB1 boundary were termed as micronuclei (**Fig. 4Dii**) while LmnB1-negative DAPI blobs close to the lamina discontinuity sites were considered as nuclear leakages (**Fig. 4Diii**). Large spherical LmnB1-positive DAPI-lobules were found in more than 10 % of the filament-containing cells. We classified these extensively deformed nuclei as fragmented or blebbed (**Fig. 4C and 4Div**). Similar nuclear blobs and lobules were observed in the detaching cells in our live cell microscopy experiments suggesting necrosis-like cell death (**Fig. 3C and Supplementary video 3**). Nuclear rupture in few Syn-filament-containing cells resulted in leakage of nuclear material into the cytoplasm which was not observed in absence of the filaments (**Fig. 4E and Supplementary video 5**).

Next, we prepared nuclear and non-nuclear fractions as depicted in **Fig. S4C**. In consistency with nuclear entry of Syn-filaments (**Fig. 4Biv**), both phosphorylated and non-phosphorylated forms of α-Synuclein increased in the soluble and insoluble nuclear fractions of 6th day PFF treated SNCA(DM)-EGFP cells (**Fig. 4F**). LmnB1 was mostly present in the insoluble nuclear fraction. Appearance of α-Synuclein bands in the same insoluble fraction after PFF treatment might indicate a possible association between insoluble LmnB1 and Syn-filaments (**Fig. 4F**). Mitochondria and ER were found to be close to the nucleus and partially co-localized with Syn-filaments (**Fig. 1F**). Non-significant increase of mitochondrial and ER proteins in the nuclear fractions of the PFF treated cells indicated entry of a small fraction of these organelle proteins into the nucleus (**Fig. 4G and S4D, Table-S4-S5**). Slight but significant drop in nuclear volume was also estimated in 6th day PFF treated SNCA(DM)-EGFP cells (**Fig. S4E**). Notably, nuclear lamina injuries were repaired with the disappearance of Syn-filaments after withdrawal of PFF seeds or doxycycline during re-plating (**Fig. 4H**).

Syn-filaments collaborate with cytoskeleton proteins to trigger Nuclear injuries

Forces transmitted through the cytoskeleton can constrict, deform, and even rupture the cell nucleus (Beaudouin, Gerlich et al., 2002, Houthaeve, Robijns et al., 2018, Lammerding & Wolf, 2016). Filamentous IBs of α-Synuclein have been reported to contain insoluble cytoskeleton proteins (Galloway et al., 1992, Mahul-Mellier et al., 2020). IBs of other amyloidogenic proteins have also been shown to destabilize both cytoskeleton and nucleoskeleton (McMurray, 2000). We hypothesized that forces mediated by altered cytoskeleton and nucleoskeleton proteins might contribute to the nuclear injuries observed in Syn-filament-containing cells.

Syn-filaments did not overlap with actin and microtubule meshwork in 6th day PFF-treated SNCA(DM)-EGFP cells (**Fig. 5A and S5A**). Type III intermediate filament protein vimentin forms a cage surrounding the canonical homeostatic IBs (Kaganovich et al., 2008). Vimentin-cages were infrequently observed encircling Syn-aggresomes in our cells (**Fig. 5B and S5B**). While large skein-like Syn-filaments were partially stained by vimentin-antibody, small filaments remained vimentin negative suggesting that cytoskeleton organization remained mostly unperturbed despite the presence of the Syn-IBs. LINC complex proteins at the inner and outer nuclear membranes bridge cytoskeleton and nucleoskeleton (Agrawal & Lele, 2019, Burke & Stewart, 2013). Large Syn-filaments were partially co-localized with inner nuclear membrane LINC complex protein Sun2 on the NE but not with outer nuclear membrane protein Nesprin-2. However, both Sun2 and Nesprin-2 staining was observed encasing the micronuclei confirming disruption of NE at the main nuclei (**Fig. 5C and S5C**).

Remarkably, colocalization between Syn-filaments and LmnB1 significantly reduced in 6th day PFF treated SNCA(DM)-EGFP cells after just 30 min incubation with microtubule destabilizer Nocodazole or actin polymerization inhibitor Cytochalasin D (**Fig. 5D**).

However, nuclear injuries were not repaired within this time-window (**Fig. 5D**). Next, we added Nocodazole and Cytochalasin D to the 3rd day PFF treated SNCA(DM)-EGFP cells and imaged the cells after 72 hr. These long-term cytoskeleton destabilizing treatments resulted in severe nuclear fragmentation, cell clumping, and cell death even in absence of PFF (**Fig. S5D-E**) but biogenesis of large Syn-filaments was still observed in PFF treated cells (**Fig. 5E**). Surprisingly, the overlap between NE and Syn-filaments was noticed in these cells and could be due to the morphological collapse of the cytoplasm on the nucleus after 72 hr cytoskeleton destabilization (**Fig. 5E and S5D**).

While actin and tubulin networks position the nucleus in the cell and maintain its morphology (Crisp, Liu et al., 2006, Davidson & Cadot, 2021, Houben, Ramaekers et al., 2007), cytoplasmic motor protein dynein exercises pulling forces on NE and aggravate NE-injuries when the lamina is weak (Penfield, Wysolmerski et al., 2018, Salina, Bodoor et al., 2002). Unlike Nocodazole and Cytochalasin D, cell and nuclear morphology was unperturbed after 72 hr treatment with dynein ATPase inhibitor Ciliobrevin D (**Fig. S5D-E)**. Intriguingly, lamina deformities and different nuclear injuries observed in PFF-treated cells were significantly reduced in presence of Ciliobrevin D although Syn-filaments remained perinuclear and partially colocalized with LmnB1 (**Fig. 5F-G**). Altogether, these experiments suggested that biogenesis of Syn-filaments was independent of cytoskeleton but actin meshwork and microtubules facilitated their association with NE. In addition, dynein pulling forces collaborate with Syn-filaments to impart mechanical stress on NE to perturb its integrity.

Does lack of nuclear integrity contribute to saturation of proteostasis in presence of Syn-filaments? To test, we transfected FlucDM-mCherry in the Ciliobrevin-D treated cells. Turnover of FlucDM-mCherry remained inefficient suggesting restoration of nuclear integrity by Ciliobrevin D was not sufficient to rescue the full proteostatic potential (**Fig.**

5H). Dynein motor activity assists cellular transcription by translocating various transcription factors to the nucleus (Herzig, Andersson et al., 2000, Mikenberg, Widera et al., 2007). Ciliobrevin D treatment prevented up-regulation of Hsp70 transcription upon heat stress even in absence of PFF (**Fig. 5I**). This eliminated the possibility of restoring Hsp70 transcription Syn-filament containing cells by counteracting Dynein motor force. Thus, saturation of proteostasis and NE-disintegrities appear to be two independent homeostatic drawbacks of having large Syn-filaments in the cell.

If dynein force ruptured the weakened nuclear lamina in Syn-filament containing cells, then improving the mechanical strength of the lamina should protect the NE from such injuries. Overexpression of LmnB1 has been shown to increase lamina stiffness and alter nuclear signalling (Ferrera, Canale et al., 2014). Further, Lamins can modulate dynein activity and counteract its pulling forces on the NE (Guo & Zheng, 2015). We transfected 5th day PFF treated SNCA(DM)-EGFP cells with a construct overexpressing LmnB1-mCherry. While we observed diffused distribution of DAPI throughout the nucleus of untransfected cells, LmnB1-mCherry over-expression compartmentalized the DAPI staining in multiple sections irrespective of the occurrence of Syn-filaments (**Fig. 5J and S5F**). Strikingly, lamina discontinuity, micronuclei and nuclear leakages disappeared after LmnB1-mCherry over-expression despite partial co-localization of the large Syn-filaments with LmnB1 was noticed even at the extranuclear space (**Fig. 5K-M**).

Syn-aggresomes, Syn-filaments, and nuclear injuries are consistent in primary neurons

Next, we isolated hippocampal neurons from E19 pre-natal C57BL/6 mice and treated with PFFs as described in Volpicelli-Daley et al (Volpicelli-Daley, Luk et al., 2014). Neurons are reported to contain multiple MTOCs both near and far to the nucleus (Kapitein &

Hoogenraad, 2015). We observed only perinuclear staining of MTOC with γ-tubulin in our experiments. Intriguingly, blobs of endogenous α-Synuclein stained with p129-Syn antibody were found to be positioned on these perinuclear γ-tubulin dots suggesting aggresome-like deposits (**Fig. 6A**). PFF treatment resulted in extensive Syn-filament formation that encaged the nucleus in these neurons. Large perinuclear Syn-filaments partially overlapped the nuclear lamina, triggered profound lamina injuries and deformed the nuclei (**Fig. 6Bii-iii**). These results validated the observations in our cell culture model and further confirmed that the biogenesis of Syn-aggresomes and Syn-filaments and the nuclear injuries triggered by Syn-filaments (i) were not exclusive to only mitotic cells, (ii) were not intrinsic properties of particular mutants of α-Synuclein and (iii) were not dependent on over-expression of exogenous α-Synuclein.

Discussion

Syn-aggresomes and Syn-filaments offer unique homeostatic potentials

Misfolding-prone proteins undergo organized aggregation into membrane-less inclusion bodies (IBs). The biogenesis principles of these PQC-deposits depend on the misfolded protein under investigation, degree of misfolding, model system being studied, etc. Here, we report two different IBs of α-Synuclein in same cells offering unique homeostatic opportunities. Perinuclear Syn-aggresomes spontaneously emerge in a cytoskeleton-driven mechanism, buffer UPS-mediated degradation of α-Synuclein, and define the rate-limiting step of its transition into Filaments (Hardenberg, Sinnige et al., 2021, Ray et al., 2020). We reduce the lag phase of soluble to filament conversion by adding recombinant α-Synuclein fibrils (PFFs) in culture. Filamentous IBs (Syn-filaments) faithfully recapitulating LB-like features appear after 6 days suggesting that seeding-based polymerization of α-Synuclein propagated through multiple cell divisions. The scattered small Syn-filaments at the initial

stages of IB-biogenesis lack ubiquitination but still do not convert into terminal IBs like IPODs. Rather, PQC factors recognize the larger IBs as insoluble waste for disposal and can clear them. Kinetics of the clearance is slower than biogenesis so that these filamentous IBs can be disintegrated and degraded only after impeding polymerization of fresh filaments.

Sequestration into both Syn-aggresomes and Syn-filaments limits the promiscuous interactions of soluble and oligomeric forms of α-Synuclein. Efficient self-polymerization of α-Synuclein into filaments avoid non-specific co-sequestration of other proteins into the insoluble proteome as found in our experiments and by others in primary neurons unless the overgrown filamentous IBs entirely engulfed membranous cell organelles (Henderson, Chung et al., 2017, Mahul-Mellier et al., 2020). Further, we observe that Syn-filaments are asymmetrically retained in one of the daughter cells without compromising mitotic division. Thus, the LB-like filamentous IBs of α-Synuclein self-sequester like passive IPODs but remain UPS-degradable like aggresomes/JUNQs, and we term these unique PQC-IBs as SInQCs – Seeding-based Inclusions for Quality Control (**Fig. 7 and S6**).

Syn-aggresomes and Syn-filaments: Homeostatic costs

Deposition of familial ALS associated mutant superoxide dismutase 1 (SOD1G93A) into aggresomes/JUNQs compromises quality control of other marginally stable proteins and potentially toxic (Weisberg et al., 2012). Forced targeting of SOD1G93A into passive deposits like IPODs restores the homeostatic functions of JUNQ and rescues cell viability. As per our results, accumulation of α-Synuclein in Syn-aggresomes does not accompany such risks; rather continuously contributes to turnover of excess protein. On the other hand, the 'artificially' seeded Syn-filaments do not serve any obligatory homeostatic purpose in mitotic cells but associate with at least two homeostatic costs. First, transient repurposing of PQC factors into the overgrown Syn-filaments competitively outweighs cellular proteostatic

control on other misfolding-prone proteins. Second, larger Syn-filaments associate with cytoskeleton and nucleoskeleton and weaken the nuclear lamina. Dynein-mediated force works on the weak sites and pulls the NE apart. These injuries may contribute to the deregulation of proteome balance in two ways. 1. By mixing of nucleo-cytoplasmic components. 2. By destabilizing chromatin architecture (de Leeuw, Gruenbaum et al., 2018, Karoutas & Akhtar, 2021) and therefore deregulating transcription of stress chaperones. Our data suggest that NE-injuries can be partially prevented by using a dynein inhibitor as well as by counteracting dynein force by over-expressing LmnB1 but this was unable to rescue protein homeostasis (**Fig. 7 and S6**).

Outlook

α-Synuclein was first detected on the nuclear envelope (NE) in 1988 but this observation was later considered as an antibody-staining artefact (Burre, Sharma et al., 2018, Maroteaux, Campanelli et al., 1988). Since then, many beneficial or deleterious outcomes of nuclear translocation of soluble α-Synuclein have been described but it's association with NE was not confirmed (Chen, Moncalvo et al., 2020, Kontopoulos, Parvin et al., 2006, Liu, Lee et al., 2011, Pinho, Paiva et al., 2019). Here, we confirm that Syn-filaments gradually encage the nucleus, partially associate with NE and trigger NE-injuries. Mitotic cells can still adapt, divide conveniently and the nuclear injuries may be repaired *via* remodelling of the NE during division (Dey & Baum, 2021, Smoyer & Jaspersen, 2014). Similar repairing opportunity is absent in post-mitotic neurons. Our findings also suggest that the widespread nuclear injuries observed in various amyloid-diseases (Gasset-Rosa, Chillon-Marinas et al., 2017, Liu, Shyu et al., 2015) may not be caused by the misfolded amyloids deposited in aggresomes but could be due to different perinuclear fibrillar IBs of the same protein.

Overall, we propose that the 'natural' biogenesis of filamentous LBs in post-mitotic neurons offers partial adaptation by self-sequestration of the excess α-Synuclein and by preventing overburdening of the cellular-PQC unless challenged by ever-accumulating proteostasis stress. Protection from large LB-mediated cellular degeneration may be possible by restricting the kinetics of fresh polymerization.

Methods

Generation of Expression Constructs

SNCA was PCR-amplified from pRK172/α-synuclein (Ahmad, Ramakrishna et al., 2006) and cloned into pcDNA4/TO-EGFP and pcDNA4/TO-mCherry (Rawat, Anusha et al., 2019) using Kpn I and Xho I (Thermo Scientific). *SNCA* variants (A30P, A53T and A30P+A53T (DM)) were prepared by site directed mutagenesis using primers in **Methods Table S1.** To generate tag-less SNCA construct, SNCA was PCR amplified from pRK172/α-synuclein and cloned into pcDNA4/TO using Kpn I and Xho I. To generate FlucDM construct, FlucDM was PCR amplified from pCI-neo FlucDM EGFP (Gupta, Kasturi et al., 2011) and cloned into pcDNA3.1-mCherry (Park, Kukushkin et al., 2013) by using Kpn I and Xba I. To prepare LmnB1 over-expressing construct, *lmnb1* gene was PCR amplified from cDNA prepared from Hek293T cells and cloned into pCDNA3.1-mCherry using Not I and Apa I. pAAV-CAG-H2B tdTomato was obtained from Addgene (Plasmid#116870, (Economo, Viswanathan et al., 2018)). For protein purification, *SNCA* and its mutants (A30P, A53T and DM) were cloned into pET-28 a (+) expression vector using the restriction enzymes Hind III and Xho I.

Protein Purification

SNCA- pET-28 a (+) constructs were transformed into *E. coli* BL21(DE3) and induced by adding 1 mM IPTG (Sigma) at 0.6 OD_{600}. The cells were pelleted 3 hr after

induction and was resuspended in TNE buffer (50 mM Tris, 150 mM NaCl, 10 mM EDTA pH 8) and frozen in – 80°C until use. Frozen cell pellets were immediately subjected to heat shock at 95°C for 10 min and centrifuged at 18,000 g. The supernatant was subjected to streptomycin and ammonium sulphate precipitation. The precipitate was dissolved in HEPES buffer (50 mM HEPES, 100 mM KCl pH 7) and size exclusion chromatography was performed using HiLoad 16/600 Superdex 75 pg Column (GE28-9893-33, GE Healthcare) attached to BioLogic DuoFlow Chromatography system (Bio-Rad). After purification, α-Synuclein and mutants were concentrated using 10 kDa Amicon (Merck Millipore) up to 4 mg/ml in HEPES buffer.

Preformed fibril (PFF) generation

The protein pellet of wild type α-Synuclein obtained after streptomycin sulfate and ammonium sulfate precipitation was dissolved in HEPES buffer 0.04 % sodium azide and subjected to size exclusion chromatography as described above. Eluted fraction was concentrated up to 1mg/ml using 10 kDa Amicon (Merck Millipore). 1 ml of concentrated protein was aliquot into 1.5 ml tubes (LoBind, Eppendorf) and kept on Eppendorf ThermoMixer C at 37°C with 1500 rpm for 48 hr. Fibril formation was checked using a small aliquote in ThT assay and the formed fibrils were sonicated using 3 mm thick probe sonicator (cat: VCX 130 PB, SONICS Vibra-Cell) for 1 min with setting: 5 second ON, 2 second OFF, 15 % amplitude. Sonicated PFF were then aliquoted into 50 and 100 µl volume and stored in – 80°C until use. The PFF stored at – 80°C were stable for 5-6 months with similar aggregation propensity in cell culture.

Thioflavin T assay

10 µM Thioflavin T (ThT) (Sigma) was added to each protein sample, aliquoted into 96-well plates, and incubated at 37°C with linear shaking at 600 rpm of diameter 1 mm in Enspire Multimode Plate Reader (Perkin Elmer) for 4 days until fluorescence reaches the saturation. Instrument was set to take fluorescence reading (Ex: 440nm Em: 480nm) at 15 min interval. Each experiment was repeated three times.

Circular Dichroism spectroscopy

For far-UV CD spectra, 10 µl of 4 mg/ml monomeric (before fibrilization) and aggregated (after fibrilization) wild type α-Synuclein and its variants were added in a 1 mm path length quartz cell (Hellma Analytics) and analyzed using a CD spectrometer (Jasco J-815) in wavelength range of 198 to 260 nm. Raw data was processed by buffer subtraction and smoothing as per the manufacturer's recommendations (Ver.1.54.03, Spectra Manager™)

Transmission Electron Microscopy (TEM)

10 µl of 4 mg/ml aggregated (after fibrilization) wild type α-Synuclein and its mutants were spotted on 300 mesh copper grid (cat: 2005C-XA, SPI supplies) and incubated at room temperature for 10 min. Thereafter, the grids were washed twice with autoclaved deionized water, and the remaining water was gently wiped off with Whatman® filter paper. This was followed by staining of all the samples with 10 µl of filtered aqueous uranyl acetate solution (2% (w/v)) for another 10 min. Finally, the grids were air-dried for 10 min. The images were acquired at 200 KV Transmission Electron Microscope (JEOL, Japan) accelerated at 200 kV.

Quantitative RT-PCR

Total RNA was prepared using NucleoSpin RNA kit (cat: 740955, Macherey-Nagel) according to the manufacturer's protocol. RNA concentration was measured using Nanodrop

2000 spectrophotometer (Thermo Scientific). For cDNA synthesis, 2 µg of total RNA was used along with SuperScript III Reverse Transcriptase (cat:18080093, Invitrogen) in a final volume of 20 µl. Quantitative PCR was carried out in Applied Biosystems 7900 HT Fast Real-Time PCR System with iTaq® Universal SYBR® Green Supermix (cat:172-5124, Bio Rad) using RT-PCR primers (**Methods Table S2**).

Cell Culture, transfection and preparation for microscopy

Hek293T and Neuro2a cells were maintained in Dulbecco's Modified Eagle's Medium (Gibco) supplemented with 10 % fetal bovine serum (FBS) (Gibco) and 90 U/ml penicillin (Sigma) 50 µg/ml streptomycin (Sigma) at 37°C and 5 % CO_2. Transfection of cells was performed with Lipofectamine 3000 reagent (Invitrogen) according to the manufacturer's protocol. For stable cell line preparation, pcDNA6/TR and pcDNA4/TO system was used (Life Technologies). 24 hr after transfection with pcDNA6/TR, 10,000 cells were seeded in a 100 mm dish and selected with 5 µg/ml Blasticidin S HCl (Invitrogen). Colonies formed after 2-3 weeks were analyzed for anti-TET repressor by western blots (data not shown). Positive clone for pcDNA6/TR was transfected with various pcDNA4/TO constructs and selected with 200 µg/ml Zeocin (Invitrogen). Surviving colonies after 2-3 weeks were tested for induction by adding 1 µg/ml Doxycycline (MP Bioscience) by fluorescence microscopy and western blot. Positive clones were frozen and/or maintained for further experiment.

For filamentous IB formation, wild type SNCA-EGFP (and other variants) stable cell lines were induced by 1 µg/ml Doxycycline for 24 hr. Next day, induced cells were trypsinized and subcultured into various dishes according to **Methods Table S3** for 6 days. 1 µM PFF and 1 µg/ml doxycycline were added after 6 hr of cell plating.

For SILAC based mass spectrometry – cells were grown in SILAC DMEM (Thermo Scientific) supplemented with 10% dialyzed FBS (Gibco), 90 U/ml penicillin (Sigma), 50

µg/ml streptomycin (Sigma) and either Light [L-Lysine 2HCl / L-Arginine HCl (Lys0/Arg0)] or Medium [L-Lysine 2HCl (4,4,5,5-D4) / L-Arginine HCl ($^{13}C_6$) (Lys4/Arg6)] or Heavy [L-Lysine 2HCl ($^{13}C_6$, $^{15}N_2$) / L-Arginine HCl ($^{13}C_6$, $^{15}N_4$) (Lys8/Arg10)] isotopes of lysine and arginine (Thermo Scientific).

For Live Cell Microscopy – Cells were grown on Lab-Tek 2-well chambered cover glass (Nunc) under normal growth condition and imaged on OLYMPUS FV3000 Laser scanning microscope at 37°C and 10 % CO_2.

For Live Cell Staining – MitoTracker™ Red CMXRos (Invitrogen) staining was done at a final concentration of 0.5 µM in culture media by incubating cells for 30 min at normal growth conditions. Slides were prepared after acetone/methanol fixation by counterstaining with DAPI (Sigma). For ER and Lysosome staining, cells grown on 2-well chambered cover glass (Nunc) were treated with 100 nM ER-Tracker™ Blue-White DPX (Invitrogen) and 1µM LysoTracker™ Red DND-99 (Invitrogen), respectively, in culture media for 30 min and taken for imaging without fixation using OLYMPUS FV3000 microscope.

Acetone/Methanol fixation – Cells grown on cover glass were washed with PBS to remove medium. Prechilled acetone and methanol in ratio 1:1 were added to the cells and plate was incubated at -20 °C for 5 mins followed by PBS wash.

Paraformaldehyde fixation –Cells were incubated with 4% paraformaldehyde solution at room temperature for 15 min followed by PBS wash. 0.1% Triton X100 in PBS was used for cell permeabilization prior to immunostaining.

Primary Neuron Culture

Hippocampal Primary neurons were isolated from E17-E19 C57BL/6 mouse brains (Charles River Laboratories) as described in Seibenhener et al (Seibenhener & Wooten, 2012) and approx. 90000 cells were cultured on poly-D-lysine coated 18 mm glass

coverslips. Neurobasal Feeding Media was replaced every third day. For Syn-filament generation, 100 nM PFF was added at 5 days *in vitro* (DIV) and incubated for 10 days at described in Volpicelli-Daley et al (Volpicelli-Daley et al., 2014). All experiments were performed in accordance with the standard protocols and procedures approved by the Institutional Animal Ethics Committee (IAEC). Primary neurons were fixed on 15 DIV with 1:1 acetone and methanol chilled at -20 °C and immune stained with appropriate antibodies.

Immunofluorescence microscopy

Cells were grown on 18 mm glass coverslips in 12 well plate (Nunc) and fixed as explained above. After fixation, blocking was done by incubating the coverslips with 5% BSA prepared in PBS with 0.05% Tween-20 (PBST) for 30 min at RT with constant shaking. Required primary antibody (**Methods Table S4**) was added and coverslips were incubated at 4°C overnight followed by PBST wash. Suitable secondary antibody was added to the coverslip and incubated for 1 hr at room temperature. Antibody dilutions were prepared in 0.1% BSA with PBST as mentioned in **Methods Table S4** Slides were prepared after DAPI staining using 10 µl Antifade Mounting Medium (cat: H-1000, Vectashield). For Actin filament staining, after fixation cells were stained with 1:1000 dilution of ActinRed™ 555 ReadyProbes™ Reagent (Rhodamine phalloidin) (cat: R37112, Thermo scientific) for 30 min at RT. Imaging was done in either Leica TCS SP8 or ZEISS LSM 880 laser scanning microscope.

Cell Viability Assay

MTT (Sigma) solution (0.5 mg/mL in growth medium) was added to cell culture plates followed by incubation for 3 hr under normal growth conditions. Media was removed and

formazan crystals were dissolved in DMSO. Absorbance was measured at 570 nm using Multiskan GO Plate Reader (Thermo Scientific).

Sample preparation and Western Blotting

Cell pellets were lysed in TBS-T lysis buffer containing 1% Triton X-100 in 50 mM Tris-HCl, 150 mM KCl, and a cocktail of protease inhibitors (Roche) at 4 °C for 1 hr with intermittent vortexing. Lysed cells were centrifuged at 12,000 g for 15 min at 4°C, and the supernatant was collected as the soluble fraction. The remaining pellet was washed twice with 1×PBS and boiled in 4×SDS loading buffer (0.2 M Tris–HCl pH 6.8, 8 % SDS, 0.05 M EDTA, 4 % 2-mercaptoethanol, 40 % glycerol, 0.8 % bromophenol blue) for 15 min to obtain the insoluble fraction. Total fraction was prepared by directly dissolving the cell pellet in 4×SDS loading buffer for 15 min. For non-nuclear, nuclear and nuclear insoluble fraction preparation, cell pellets were processed using NE-PER Nuclear and Cytoplasmic Extraction Kit (cat:78833, Thermo Scientific). Protein fraction concentration was estimated by Amido Black Protein estimation assay.

Protein fractions were separated by SDS-PAGE and transferred onto 0.2 μm PVDF membrane (Bio-Rad) for 90 min at 300 mA using the Mini-Trans Blot cell system (Bio-Rad). Membranes were probed by appropriate primary and secondary antibodies (**Methods Table S4**) and imaged using documentation system (Chemi-Smart 5000, Vilber Lourmat).

Sample Preparation for Mass Spectrometry

For total, soluble and insoluble proteome, cells were prepared according to the experimental scheme in **Fig. S3C**. Cells were pelleted down at day 3 and day 6, respectively. Equal number (~1 million) of L-, M-, and H-labeled cells were pooled together for the preparation of the fractions and were separated on NuPAGE 4%–12% Bis–Tris Protein Gels

(Invitrogen). The gel was run in MES buffer (100 mM MES, 100 mM Tris–HCl, 2 mM EDTA, 7 mM SDS) at 200 V for 40 min, fixed and stained with Coomassie brilliant blue. Preparation of gel slices, reduction, alkylation, and in-gel protein digestion was carried out as described by Shevchenko et al. (Shevchenko, Wilm et al., 1996). Finally, peptides were desalted and enriched according to Rappsilber et al. (Rappsilber, Ishihama et al., 2003) and stored in -20°C until Mass spectrometry analysis. Similarly, equal number (~ 1.5 million) of L- and H-labeled cells were pooled together to prepare non-nuclear, nuclear and nuclear insoluble fraction as explained in experimental scheme in **Fig. S4C**.

Peptides eluted from desalting tips were dissolved in 2% formic acid and sonicated for 5 min. Peptides were then analyzed on Q Exactive HF (Thermo Scientific) mass spectrometer interfaced with nano- flow LC system (EASY-nLC 1200, Thermo Scientific). EasySpray Nano Column PepMap^{TM} RSLC C18 (Thermo Fisher) (75 μm× 15 cm; 3 μm; 100 Å) using 60 min gradient of mobile phase [5% ACN containing 0.1% formic acid (buffer A) and 90% ACN (acetonitrile) containing 0.1% formic acid (buffer B)] at flow rate 300 nL/min was used for separation of peptides. Full scan of MS spectra (from m/z 400 to 1750) were acquired followed by MS/MS scans of top 10 peptide with charge state 2 of higher. The MS-based proteomics data of all these experiments have been deposited to the ProteomeXchange Consortium via the PRIDE partner repository (Vizcaino, Deutsch et al., 2014) with the dataset identifier PXD028941.

Peptide Statistics

For peptide identification, raw MS data files were loaded onto MaxQuant proteomics computational platform (Ver. 1.6.10.43) (Cox & Mann, 2008) and searched against Swissprot database of Homo sapiens (release 2019 with 20,371 entries) and a database of known contaminants. MaxQuant used a decoy version of the specified database to adjust the false

discovery rates for proteins and peptides below 1%. The search parameters included constant modification of cysteine by carbamidomethylation, enzyme specificity trypsin, and multiplicity set to 3 with Lys4 and Arg6 as medium label and Lys8 and Arg10 as heavy label. Other parameters included minimum peptide for identification 2, minimum ratio count 2, re-quantify option selected, and match between runs with 2-min time window.

Downstream analysis and statistics of normalized ratios (H/L and M/L) from two biological repeat experiments was done using Perseus (Ver. 1.6.0.4, 1.6.10.43) (Tyanova, Temu et al., 2016). Individual experiment H/L ratios for each fraction were converted into log2 space and one-sample t-test was performed to calculate the statistical significance with Perseus. For Z-score calculation, average ratio H/L of 2 repeats was converted into log2 space and normalized using mean and standard deviations for each data set in Perseus. Heatmaps were prepared using Morpheus (https://software.broadinstitute.org/morpheus) and other graphs were prepared either in Perseus or using OriginPro 2021b (OriginLab).

Methods Table S1 - Cloning Primers			
Gene Name	**Primer Sequence**	**Source**	**Catalog**
SNCA	Forward – GCGGTACCATGGATGTATTCATGAAAGG	Bioserve	NA
	Reverse – CTCGAGTATGGCTTCAGGTTCGTAGTCTTG	Bioserve	NA
SNCA_A30P	Forward – GTGTGGCAGAAGCACCAGGAAAGACAAAAGAGG	Bioserve	NA
	Reverse – CCTCTTTTGTCTTTCCTGGTGCTTCTGCCACAC	Bioserve	NA
SNCA_A53T	Forward – GTGCATGGTGTGACAACAGTGGCTGAGAAG	Bioserve	NA
	Reverse – CTTCTCAGCCACTGTTGTCACACCATGCAC	Bioserve	NA
SNCA_Stop	Forward – GCGGTACCATGGATGTATTCATGAAAGG	Bioserve	NA
	Reverse – CCTCTAGACTCGAGTTAGGCTTCAGGTTCGTAG	Bioserve	NA

FlucDM	Forward – GGTACCATGGAAGACGCCAAAAACAT	Bioserve	NA
	Reverse – GGATCCCGGGTTTCACGGCGATC	Bioserve	NA
Lamin B1	Forward – CAGTGGCGGCCGCATGGCGACTGCGACCCCCGTGCC	Bioserve	NA
	Reverse – GGTTTAAACGGGCCCTTACATAATTGCACAGCTTCTATTGG	Bioserve	NA

Methods Table S2 - Quantitative RT-PCR Primers			
Gene Name	**Primer Sequence**	**Source**	**Catalog**
HSPA1A	Forward - CAAGGCCCAGATTCACGACC	Bioserve	NA
	Reverse - GATCTGCGTCTGCTTGGTGG	Bioserve	NA
GAPDH	Forward - CGATGCTGGCGCTGAGTACG	Bioserve	NA
	Reverse - GCAGTTGGTGGTGCAGGAGG	Bioserve	NA

Methods Table S3 – Cell Number		
Format	**Media (ml)**	**Cell number**
12-well plate (Nunc)	1	5,000
6-well plate (Nunc)	2	10,000
60mm dish (Nunc)	3	15,000
100mm dish (Nunc)	10	1,00,000
2-chambered cover glass (Nunc)	1	5,000

Methods Table S4 - Antibody List				
Primary Antibody				
Antibody Name	**Company**	**Catalog number**	**Dilution**	
			ICC	**Western**
Rabbit Monoclonal, alpha Synuclein Antibody (14H2L1)	Invitrogen	701085	1:1000	1:10,000
Rabbit Monoclonal, Anti-Alpha-synuclein (phospho S129) Antibody [MJF-R13 (8-8)]	abcam	ab168381	1:1000	1:10,000
Mouse Monoclonal, Anti-alpha synuclein (Phospho S129) Antibody (P-syn/81A)	abcam	ab184674	1:500	NA
Mouse monoclonal, Ubiquitin (P4D1) Antibody	santa cruz biotec.	sc-8017	1:500	1:5000
Rabbit polyclonal, SQSTM1(P62) Antibody	Invitrogen	PA5-27247	1:100	NA
Rabbit Polyclonal, LC3B Antibody	abcam	ab51520	1:500	NA
Mouse Monoclonal, Gamma-Tubulin (4D11) Antibody	Invitrogen	MA1-850	1:100	NA
Rabbit Monoclonal, Lamin B1 Antibody	Invitrogen	PA5-19468	1:1000	1:10,000
Rabbit Monoclonal, Vimentin (D21H3) XP Antibody	Cell signaling	5741	1:250	NA
Rabbit Polyclonal, UNC84B Antibody	Invitrogen	PA5-95741	1:250	NA
Rabbit Polyclonal, Nesprin 2 Antibody	Invitrogen	PA5-62155	1:250	NA
Rabbit Polyclonal, Firefly Luciferase Antibody	abcam	ab21176	NA	1:10,000

Rabbit Polyclonal, Tet Repressor Antibody	Invitrogen	PAI-29677	NA	1:5000
Mouse monoclonal, Beta Actin antibody	abcam	ab8224	NA	1:10,000
Rabbit polyclonal, Beta Tubulin Antibody	abcam	ab6046	1:500	1:10,000
Mouse monoclonal, GAPDH [6C5] antibody	abcam	ab8245	NA	1:10,000
Secondary Antibody				
Anti-Rabbit IgG (Whole molecule) (peroxidase conjugate)	sigma	A6154	NA	1:20,000
Anti-mouse IgG (whole molecule) (peroxidase conjugate)	sigma	A4416	NA	1:20000
Goat anti-Rabbit IgG (H+L) Highly Cross-Adsorbed Secondary Antibody, Alexa Fluor 488	Invitrogen	A11034	1:1000	NA
Goat anti-Mouse IgG (H+L) Cross-Adsorbed Secondary Antibody, Alexa Fluor 488	Invitrogen	A11001	1:500	NA
Goat anti-Rabbit IgG (H+L) Cross-Adsorbed Secondary Antibody, Alexa Fluor 647	Invitrogen	A21244	1:1000	NA
Goat anti-Mouse IgG (H+L) Highly Cross-Adsorbed Secondary Antibody, Alexa Fluor Plus 647	Invitrogen	A32728	1:500	NA
Goat anti-Rabbit IgG (H+L) Cross-Adsorbed Secondary Antibody, Alexa Fluor 555	Invitrogen	A21428	1:1000	NA

Figure 1

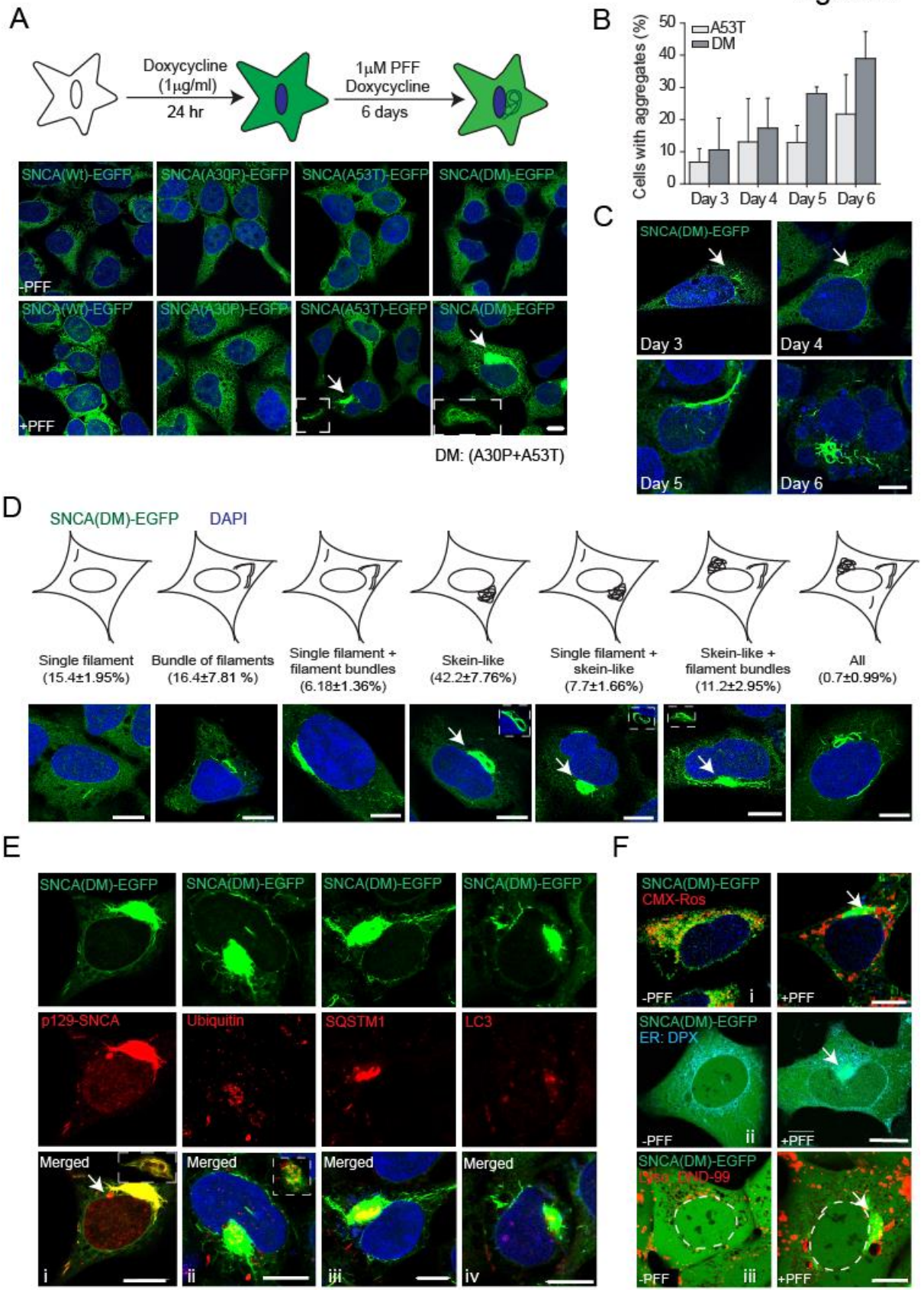
A
Doxycycline
(1μg/ml)
24 hr
1μM PFF
Doxycycline
6 days
SNCA(Wt)-EGFP
SNCA(A30P)-EGFP
SNCA(A53T)-EGFP
SNCA(DM)-EGFP
-PFF
+PFF
DM: (A30P+A53T)
B
Cells with aggregates (%)
A53T
DM
Day 3
Day 4
Day 5
Day 6
C
SNCA(DM)-EGFP
Day 3
Day 4
Day 5
Day 6
D
SNCA(DM)-EGFP
DAPI
Single filament
(15.4±1.95%)
Bundle of filaments
(16.4±7.81 %)
Single filament +
filament bundles
(6.18±1.36%)
Skein-like
(42.2±7.76%)
Single filament +
skein-like
(7.7±1.66%)
Skein-like +
filament bundles
(11.2±2.95%)
All
(0.7±0.99%)
E
SNCA(DM)-EGFP
p129-SNCA
Ubiquitin
SQSTM1
LC3
Merged
i
ii
iii
iv
F
SNCA(DM)-EGFP
CMX-Ros
ER: DPX
Nuc: DND-99
-PFF
+PFF

Fig. 1: A cell culture model recapitulating filamentous inclusions of α-Synuclein.

A: Top**:** Experimental scheme. Bottom: Hek293T stable lines expressing EGFP-tagged α-Synuclein (SNCA) variants. Cells were imaged at 6th day in presence or absence of PFF. Arrows indicate IBs. Insets: low exposure images of the indicated IBs.

B: Number of SNCA(A53T)-EGFP and SNCA(DM)-EGFP cells with IBs during the course of PFF-incubation. Approx. 100 cells have been counted in each experiment. N = 3.

C: Different stages and localization of Syn-IBs in SNCA(DM)-EGFP cells at different days during the course of PFF-incubation.

D: Morphology of Syn-IBs in 6th day PFF-treated SNCA(DM)-EGFP cells with percent distribution. Approx. 100 cells have been counted in each experiment. N = 3. Insets – low exposure images of the arrow-indicated IBs.

E: 6th day PFF-treated SNCA(DM)-EGFP cells were immunostained with markers for canonical LBs and imaged. Insets – low exposure images of the IBs. Arrow in **Ei** indicate a separate blob stained by p129-Syn antibody.

F: 6th day PFF-treated SNCA(DM)-EGFP cells were stained for various cell organelles and imaged. Dashed circles indicate nuclear boundary in **Fiii**.

Error bars indicate standard deviation from at least three independent experiments. Blue staining in microscopy images indicate nucleus (DAPI). Scale bar – 10 μm. All cells are fixed using acetone-methanol method for microscopy except panel **Fii-iii** where live cells stained with ER-tracker and Lyso-Tracker were imaged.

Figure S1

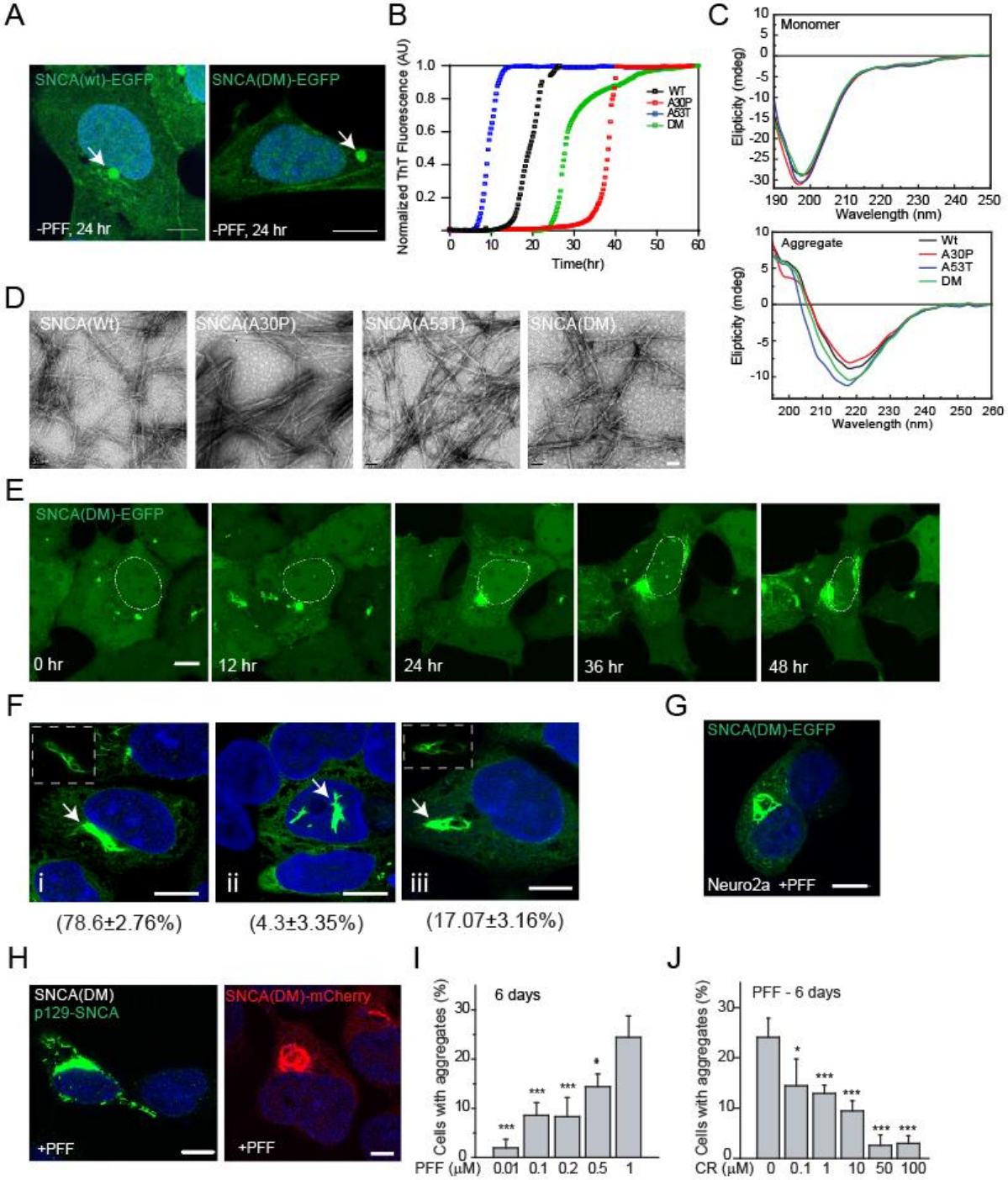
A
SNCA(wt)-EGFP
-PFF, 24 hr
SNCA(DM)-EGFP
-PFF, 24 hr
B
Normalized ThT Fluorescence (AU)
Time(hr)
WT
A30P
A53T
DM
C
Monomer
Ellipticity (mdeg)
Wavelength (nm)
Aggregate
Wt
A30P
A53T
DM
D
SNCA(Wt)
SNCA(A30P)
SNCA(A53T)
SNCA(DM)
E
SNCA(DM)-EGFP
0 hr
12 hr
24 hr
36 hr
48 hr
F
i
ii
iii
(78.6±2.76%)
(4.3±3.35%)
(17.07±3.16%)
G
SNCA(DM)-EGFP
Neuro2a +PFF
H
SNCA(DM)
p129-SNCA
+PFF
SNCA(DM)-mCherry
+PFF
I
6 days
Cells with aggregates (%)
PFF (μM) 0.01 0.1 0.2 0.5 1
J
PFF - 6 days
Cells with aggregates (%)
CR (μM) 0 0.1 1 10 50 100

Fig. S1: A cell culture model recapitulating filamentous inclusions of α-Synuclein.

A: Hek293T stable lines expressing EGFP-tagged α-Synuclein (SNCA) variants. Cells were fixed for microscopy using paraformaldehyde. Scale bar – 10 μm.

B: Thioflavin T assay for α-Synuclein (SNCA) variants.

C: Far UV CD spectra of the α-Synuclein (SNCA) variants.

D: Transmission electron microscopy (TEM) images of the fibrils generated by the α-Synuclein (SNCA) variants *in vitro*. Scale bar – 50 nm.

E: Live cell microscopy showing Syn-filaments at different stages of biogenesis. Imaging started at 4th day of the experimental scheme shown in **Fig. 1A**. Dashed circles indicates nuclear boundary. Scale bar – 10 μm.

F: Localization of Syn-filaments in 6th day PFF-treated SNCA(DM)-EGFP cells with percent distribution. Approx. 100 cells have been counted in each experiment. N = 3. Insets – low exposure images of the arrow-indicated IBs.

G: Neuro2a stable line expressing SNCA(DM)-EGFP. Cells were treated with PFF for 6 days and fixed for microscopy using acetone-methanol. Scale bar – 10 μm.

H: Hek293T stable lines expressing SNCA(DM) and SNCA(DM)-mCherry. Cells were treated with PFF for 6 days and fixed for microscopy using acetone-methanol. SNCA(DM) cells were immunostained with p129-Syn (MJF-R13 (8-8)) antibody. Scale bar – 10 μm.

I: Hek293T stable line expressing SNCA(DM)-EGFP was treated with different concentrations of PFF for 6 days; number of Syn-filament containing cells were counted and plotted. Approx. 150 cells have been counted in each experiment. N = 3

J: Hek293T stable line expressing SNCA(DM)-EGFP treated with 1 μM PFF and varied concentration of Congo Red (CR) for 6 days. Number of aggregate containing cells were counted and plotted. Approx. 200 cells were counted in each experiment. N = 3

Error bar indicates the standard deviation from at least 3 independent experiments. p-value<0.005 = ***, and p-value 0.05= *, Student's *t*-test.

Figure 2

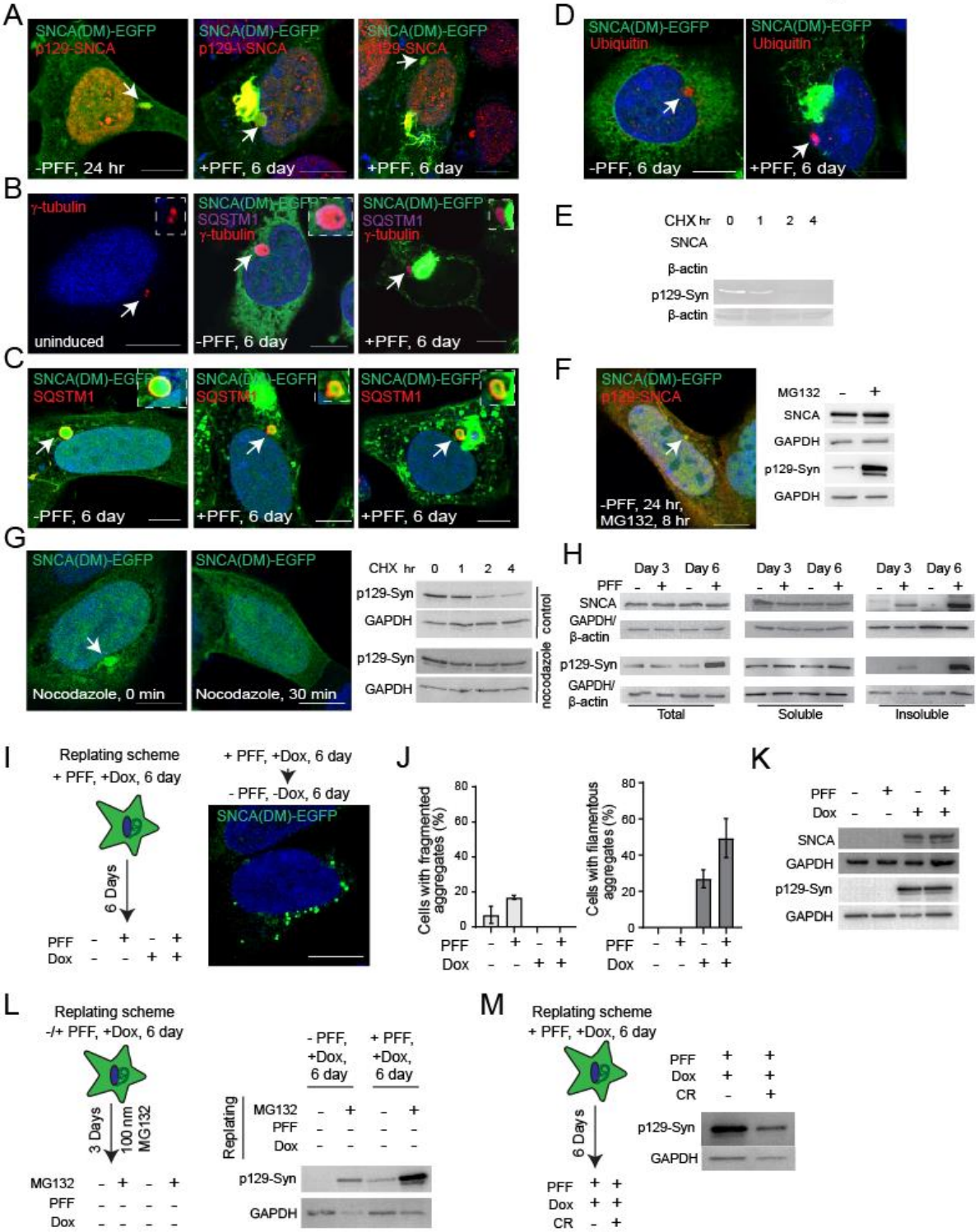

Fig. 2: Syn-filaments and Syn-Aggresomes.

A: SNCA(DM)-EGFP cells were immunostained with p129-Syn antibody (MJF-R13 (8-8), epitope: phosphoserine 129).

B: Uninduced and dox-induced SNCA(DM)-EGFP cells were immunostained with SQSTM1 and γ-tubulin antibodies. Insets: zoomed images of the arrow indicated locations.

C: SNCA(DM)-EGFP cells were immunostained with SQSTM1 antibody. Insets – zoomed images of the arrow indicated locations.

D: SNCA(DM)-EGFP cells were immunostained with ubiquitin antibody.

E: 24 hr induced SNCA(DM)-EGFP cells were treated with cycloheximide (CHX, 5 mM) for the indicated time points, total cell extract was prepared and probed with SNCA antibodies. SNCA - detecting both phosphorylated and non-phosphorylated α-Synuclein (14H2L1; epitope:117-125) and p129-Syn - detecting only phosphorylated α-Synuclein (MJF-R13 (8-8)). β-actin as loading control.

F: Left: 24 hr induced SNCA(DM)-EGFP cells were treated with MG132 (5 μM) for 8 hr and immunostained with p129-SNCA antibody. **Right**: total cell extract was prepared from the same cells immunoblotted for SNCA and p129-Syn. GAPDH as loading control.

G: Left: 24 hr induced SNCA(DM)-EGFP cells were imaged in presence and absence of Nocodazole (0.1ug/ml, for 30 min) and imaged. **Right**: same cells were treated with cycloheximide (CHX, 5 mM) for indicated time points for total fraction preparation and immunoblotted for p129-Syn. GAPDH as loading control.

H: SNCA(DM)-EGFP cells were incubated with PFF for indicated days; total, soluble and insoluble extracts were prepared as described in **Fig. S2F**, and probed for SNCA and p129-Syn. GAPDH as loading control for total and soluble fractions, β-actin for insoluble fraction.

I: Left: re-plating experiment strategy. 6th day filament containing cells were re-plated with or without doxycycline and PFF. **Right**: microscopic image of a re-plated cell. Re-plating conditions indicated.

J: Number of SNCA(DM)-EGFP cells with fragmented or filamentous IBs after 6 days of re-plating. Approx. 100 cells have been counted in each experiment. N = 3.

K: Re-plated cells were lysed and immunoblotted for SNCA and p129-Syn. GAPDH as loading control.

L: Left: experimental strategy. PFF untreated and treated 6th day cells were re-plated and 100 nM MG132 was added at every 24 hr for 3 days. **Right**: Total cell extract was prepared and probed for p129-Syn. GAPDH as loading control.

M: **Left**: experimental strategy. 6th day filament containing cells were re-plated with doxycycline and PFF in presence or absence of Congo Red. **Right**: Total cell extract was prepared and probed for p129-Syn. GAPDH as loading control.

Error bars indicate standard deviation from at least three independent experiments. Cells were fixed for microscopy with either paraformaldehyde (**A, C, F and G**) or acetone-methanol (**B, D and I**). Scale bar – 10 μm.

Figure S2

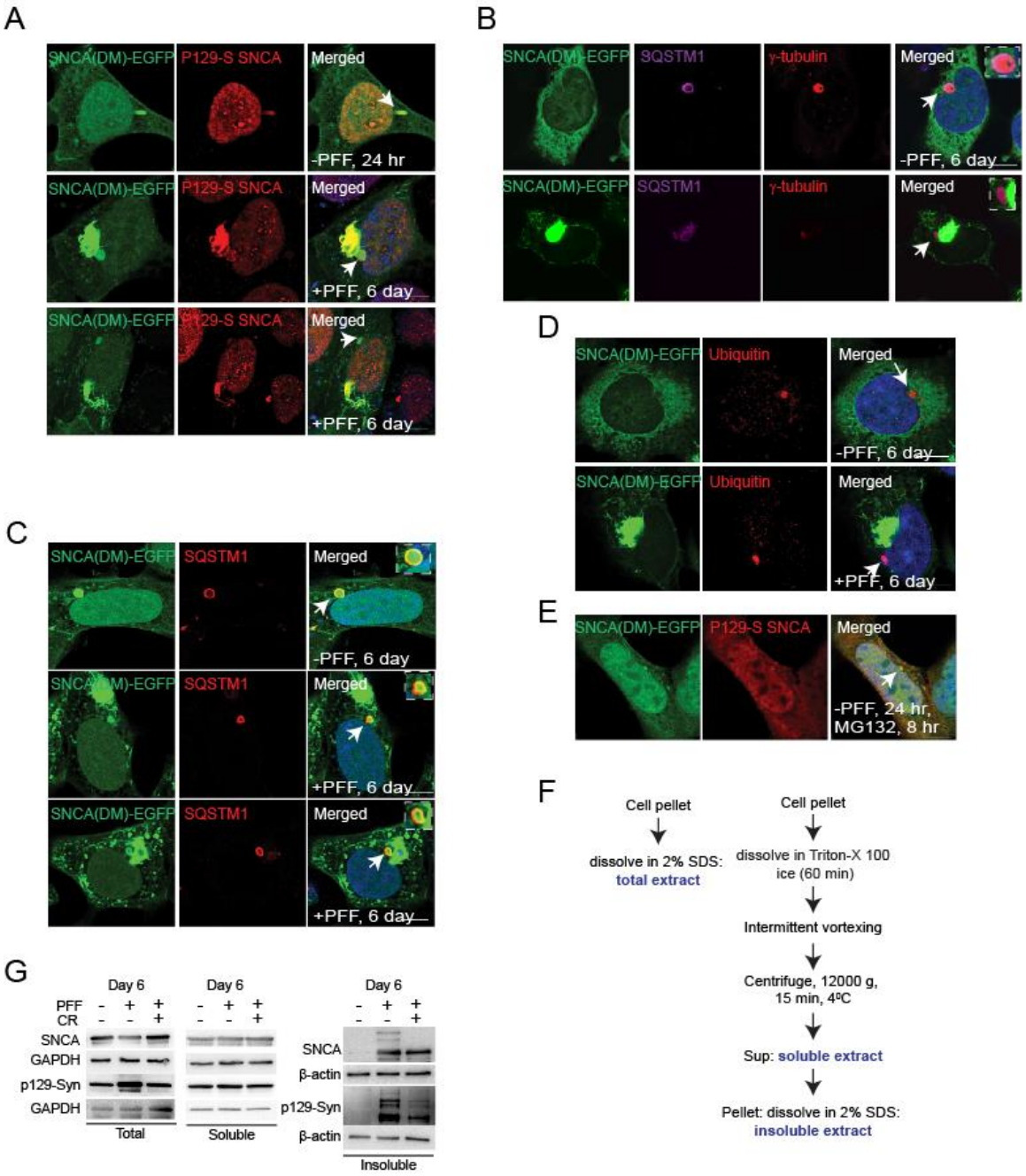

Fig. S2: Syn-filaments and Syn-Aggresomes.

A -E: Microscopic images shown in **Fig. 2A, 2B, 2C, 2D, and 2F** – images of fluorescent proteins/antibodies excited by different wavelengths of lasers are shown separately. Scale bar – 10 μm.

F: Schematic describing the experimental strategies to prepare total, soluble and insoluble cell extracts.

G: Total, soluble and insoluble fraction prepared from 6th day HEK293T SNCA(DM)-EGFP cells with indicated treatments and probed for SNCA and p129-Syn. GAPDH and β-actin as loading control.

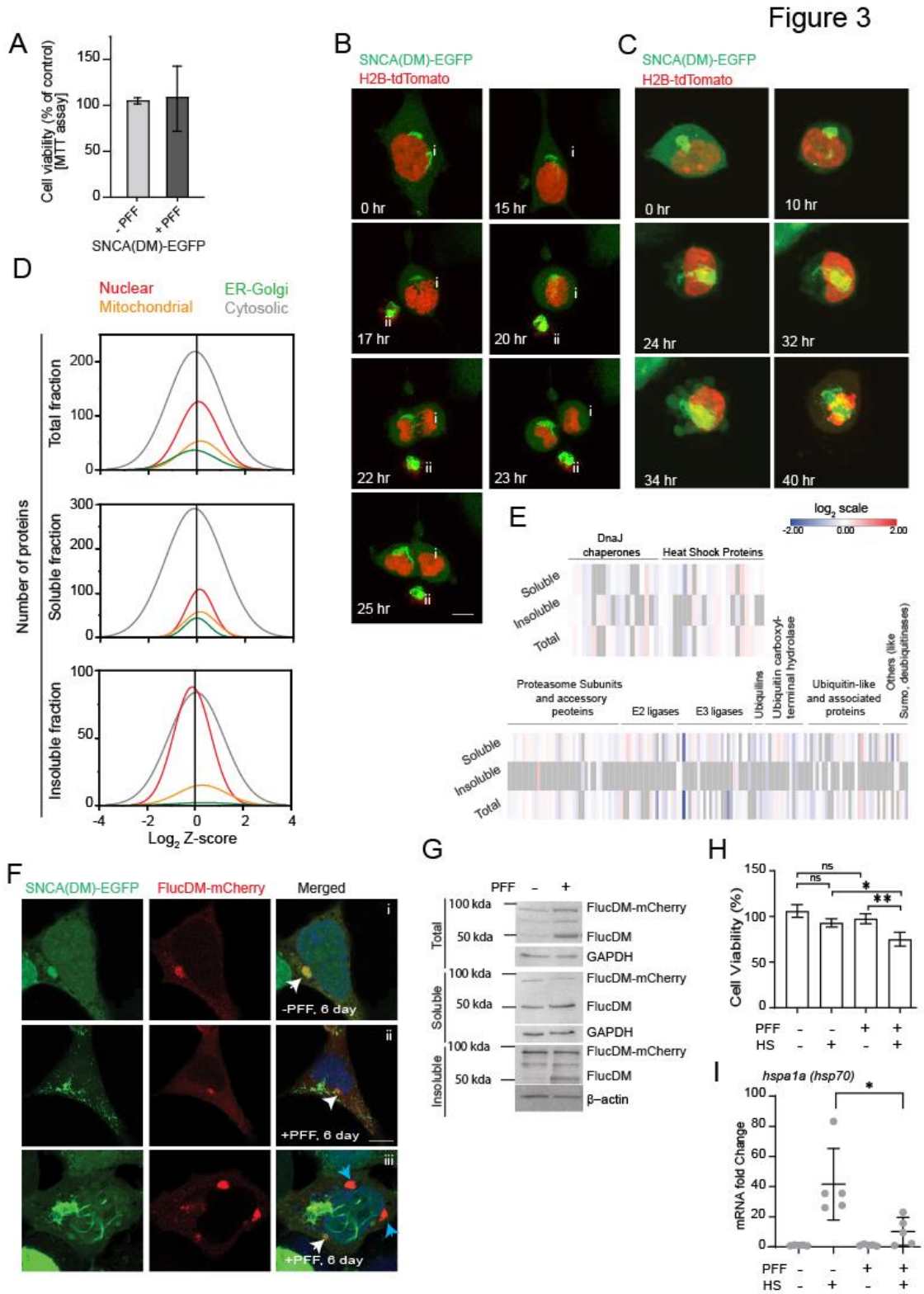

Fig. 3: Syn-filaments and cellular homeostasis

A: Cell viability of 6th day PFF treated SNCA(DM)-EGFP cells as estimated by MTT assay. Error bars indicate SDs from at least three independent experiments.

B: Different stages of mitotic division of Syn-filament containing cell as captured by live cell microscopy (**i**). A detached floating cell shown in (**ii**).

C: Detachment of Syn-filament containing cell from plate surface as captured by live cell microscopy.

D: Z-score (SNCA(DM)-EGFP; 6th day, Ratio: +PFF/-PFF) distribution of proteins identified by mass spectrometry according to their subcellular localization (as curated by Uniprot) in total, soluble and insoluble fractions. Experimental scheme presented in **Fig. S3C**.

E: Heatmap showing fold-change (SNCA(DM)-EGFP, 6day; Ratio: +PFF/-PFF) distribution of PQC-proteins in total, soluble and insoluble fractions. Experimental scheme in **Fig. S3C**.

F: Localization of FlucDM-mCherry in 6th day PFF treated and untreated SNCA(DM)-EGFP cells. Cells were transfected with FlucDM-mCherry on 5th day of incubation (**Fig 1A**).

G: Total, soluble and insoluble extracts were prepared from cells shown in **3F** and probed using Luciferase antibody. Higher ~100 kDa band corresponds to full length FlucDM-mCherry while 50 kDa band is FlucDM. GAPDH/ β-actin as loading control.

H: MTT assay - 6th day SNCA(DM)-EGFP cells with/without PFF incubation after 1hr heat shock at 42°C. N=5, * indicates p-value < 0.05, ** indicates p-value <0.005 Student's *t*-test.

I: 6th day SNCA(DM)-EGFP cells treated with HS – heat stress at 42°C for 2 hr. cDNA was prepared and RT-PCR was performed for *HSPA1A*. Fold change compared to GAPDH control is plotted. * Indicates p-value < 0.05. Welch *t*-test.

Scale bar – 10 μm.

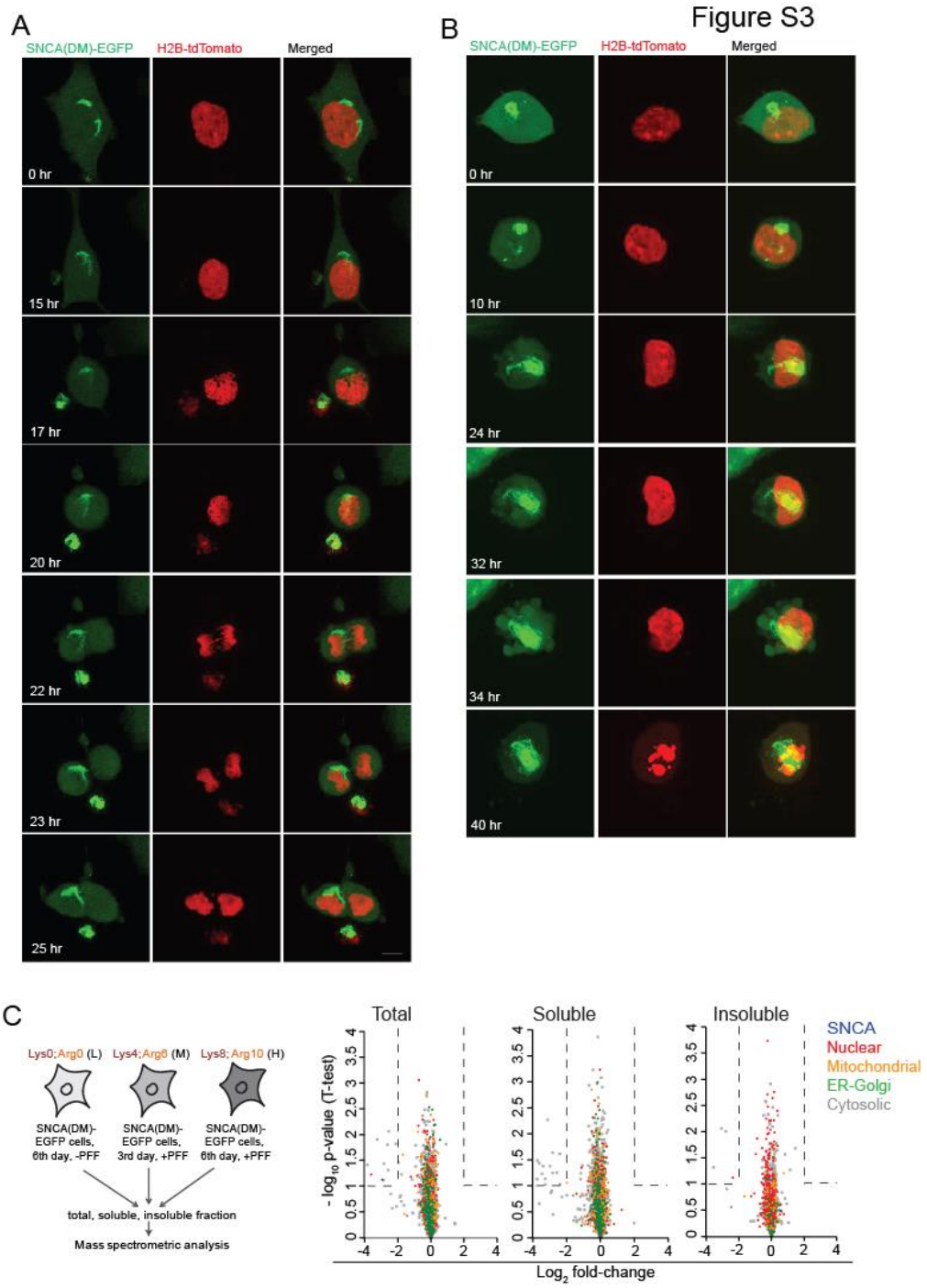

Fig. S3: Syn-filaments and cellular homeostasis

A-B: Live cell microscopic images shown in **Fig. 3B-C** – images of fluorescent proteins excited by different wavelengths of lasers are shown separately. Scale bar – 10 μm.

C: Left: Experimental scheme for **Fig. 3D**. **Right:** Volcano plot illustrating proteome equilibrium in 6th day PFF treated SNCA(DM)-EGFP cells. The $-\log_{10}$ (p-value, One-sample *t*-test) is plotted against the $\log_2$ (fold change: SNCA(DM)-EGFP; 6th day +PFF/-PFF).

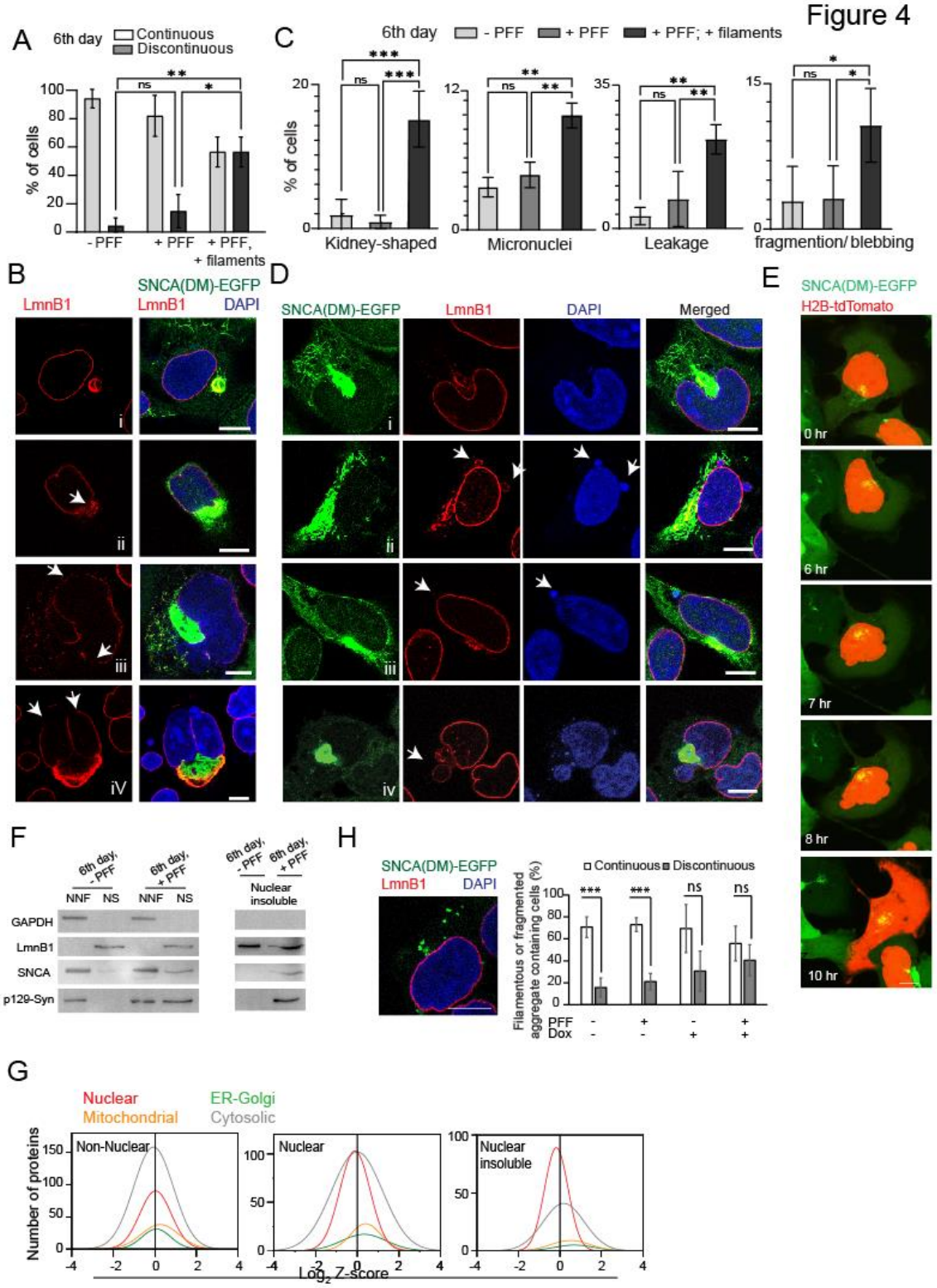

Fig. 4: Nuclear injuries in Syn-filament containing cells.

A-B: 6th day PFF treated SNCA(DM)-EGFP cells were immunostained for LmnB1.

Percentage of cells with continuous or discontinuous lamina as per LmnB1 staining plotted

(**A**). Error bar represents the standard deviation from five biological repeats. Approximately 100 cells were counted in each biological repeat. Representative images are shown (**B**). Arrows indicate irregularities in LmnB1 staining. * = p-value < 0.05 and ** = p-value <0.005, Two-way ANOVA. Scale bar – 10 μm.

C-D: 6th day PFF treated SNCA(DM)-EGFP cells were immunostained for LmnB1. Deformities of nuclear morphology and appendages as per LmnB1 and DAPI staining plotted (**C**) Error bar represents the standard deviation from five biological repeats. Approximately 100 cells were counted in each biological repeat. Representative images are shown (**D**). Arrows indicate nuclear deformity sites. * = p-value < 0.05, ** = p-value <0.005 and ***= p-value <0.001, One-way ANOVA. Scale bar – 10 μm.

E: Live cell microscopic images showing cellular localization and distribution of SNCA(DM)-EGFP and H2B-tdTomato in Syn-filament containing cells over time. Cells were transfected with H2B-tdTomato on 3rd day of PFF incubation. Scale bar – 10 μm.

F: Non-Nuclear (NNF), Nuclear soluble (NS) and Nuclear insoluble fractions were prepared from 6th day SNCA(DM)-EGFP cells (+/- PFF) and probed for LmnB1 as nuclear marker, GAPDH as cytosolic marker and p129-Syn. Fractionation procedure shown in Fig-**S4C**.

G: Z-score (SNCA(DM)-EGFP, 6th day; Ratio:+PFF/-PFF) distribution of proteins identified by mass spectrometry according to their subcellular localization (as curated by Uniprot) in Non-Nuclear, Nuclear and Nuclear insoluble fractions. Experimental scheme explained in **Fig. S4C**

H: Left: LmnB1 staining after 6th day of re-plating. Re-plating scheme same as **Fig. 2I**.

Right: Continuous or discontinuous lamina as per LmnB1 staining was estimated in fragmented or filamentous IB containing cells and plotted. Error bars indicate SDs from at least three independent experiments. ***= p-value <0.001, Student's *t*-test. Scale bar – 10 μm.

Figure S4

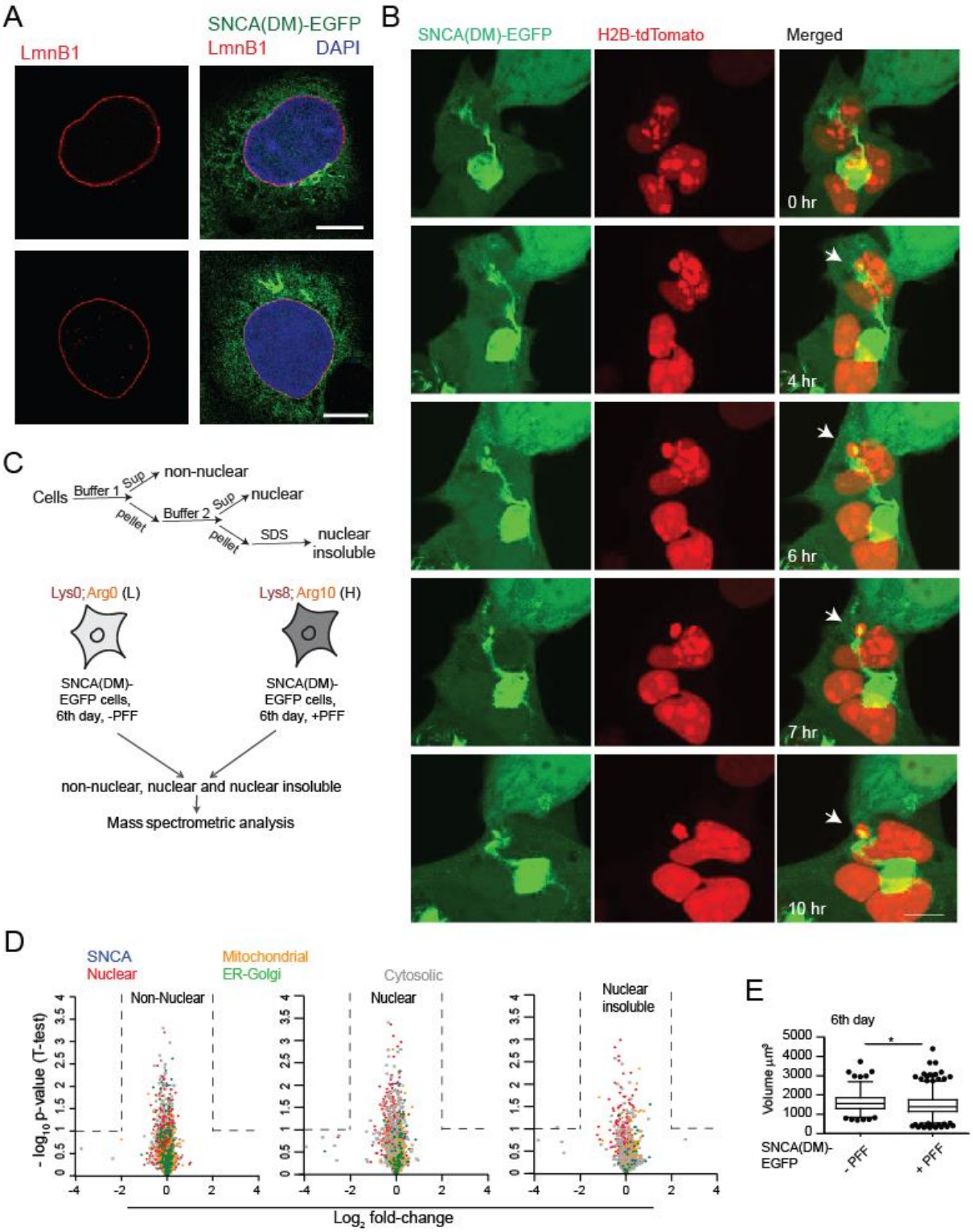

Fig. S4: Nuclear injuries in Syn-filament containing cells.

A: 6th day PFF treated SNCA(DM)-EGFP cells were immunostained for LmnB1. Localization of Syn-filaments and LmnB1 staining shown.

B: Live cell microscopy images showing nuclear deformities. SNCA(DM)-EGFP cells were transfected with H2B-tdTomato on 3rd day of PFF incubation. Arrows indicate deformity site. Scale bar – 10 μm.

C: Experimental strategy for Non-Nuclear, Nuclear soluble and Nuclear insoluble fraction preparation.

D: Volcano plot of 6th day PFF treated SNCA(DM)-EGFP cells. The $-\log_{10}$ (p-value, One-sample *t*-test) is plotted against the $\log_2$ (fold change: SNCA(DM)-EGFP; 6th day +PFF/-PFF) of Non-Nuclear, Nuclear and Nuclear pellet fraction.

E: Nuclear volume as estimated by Imaris 8.4 (Bitplane) in 6th day SNCA(DM)-EGFP cells. * indicates p-value < 0.05, Mann-Whitney U test.

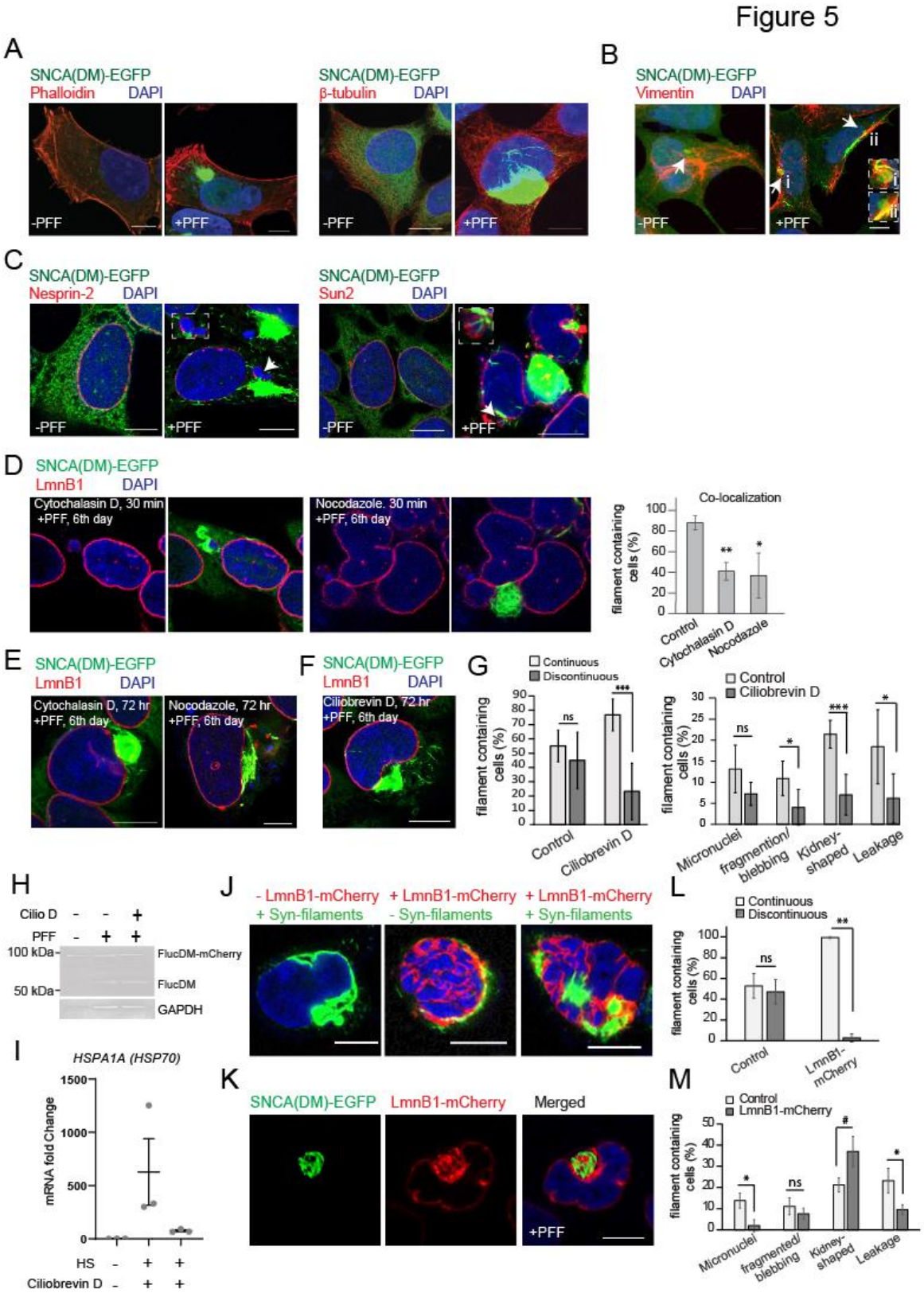

Fig. 5: Cytoskeleton, Nucleoskeleton, Perinuclear Syn-filaments and Nuclear injuries.

A: Maximum Intensity projection (MIP) of microscopic images of 6th day PFF treated SNCA(DM)-EGFP cells stained with Phalloidin-red and β-tubulin antibody.

B: Maximum Intensity projection (MIP) of microscopic images of 6th day PFF treated SNCA(DM)-EGFP cells immunostained with vimentin antibody. Arrows indicate sites of perinuclear Syn-aggresomes. Insets – zoomed images of site **i** and **ii**.

C: Microscopic images of 6th day PFF treated SNCA(DM)-EGFP cells immunostained with Nesprin-2 and Sun2 antibody. Insets – zoomed images of arrow indicated sites.

D: Left: 6th day PFF treated SNCA(DM)-EGFP cells immunostained with LmnB1. Cells were treated with Nocodazole (0.1μg/ml) and Cytochalasin D (1μg/ml) for 30 min. **Right**: Percentage of cells with LmnB1 co-localization is plotted. Control – DMSO-treated cells. Error bars represent standard deviation from three biological repeats.

E: 6th day PFF treated SNCA(DM)-EGFP cells immunostained with LmnB1. Cells were treated with Nocodazole (0.1μg/ml) and Cytochalasin D (1μg/ml) for 72 hr.

F: 6th day PFF treated SNCA(DM)-EGFP cells were immunostained for LmnB1 after 72 hr Ciliobrevin D treatment (5 μM).

G: Left: Quantification of continuous or discontinuous lamina as per LmnB1 staining after 72 hr Ciliobrevin D treatment (5 μM). **Right:** Quantification of deformities of nuclear morphology as per LmnB1 staining after 72 hr Ciliobrevin D treatment (5 μM). Control – DMSO-treated cells. Error bars represent standard deviation from five biological repeats Approx. 60 cells were counted in each experiment.

H: Total extracts prepared from 6th day cells after 72 hr Ciliobrevin D treatment as described, FlucDM-mCherry transfected on 5th day and probed using Luciferase antibody. GAPDH as loading control.

I: SNCA(DM)-EGFP cells treated with Ciliobrevin D for 72 hr and subjected to HS on 6th day. HS – heat stress at 42°C for 2 hr. cDNA was prepared and RT-PCR was performed for *HSPA1A*. Fold change compared to control is plotted.

J-K: 6th day PFF treated SNCA(DM)-EGFP cells were imaged after transfection with LmnB1-mCherry on 5th day.

L: PFF treated SNCA(DM)-EGFP cells were transfected with LmnB1-mCherry on 5th day and imaged on 6th day. Continuous or discontinuous lamina as per LmnB1-mCherry staining plotted. Approx. 50 cells have been counted in each experiment. N=3.

M: PFF treated SNCA(DM)-EGFP cells were transfected with LmnB1-mCherry on 5th day and imaged on 6th day. Deformities of nuclear morphology and appendages as per LmnB1-mCherry and DAPI staining plotted. Approx. 50 cells have been counted in each experiment. N=3.

Scale bar – 10 μm. * = p-value < 0.05 and ** = p-value <0.005, Student's *t*-test.

Figure S5

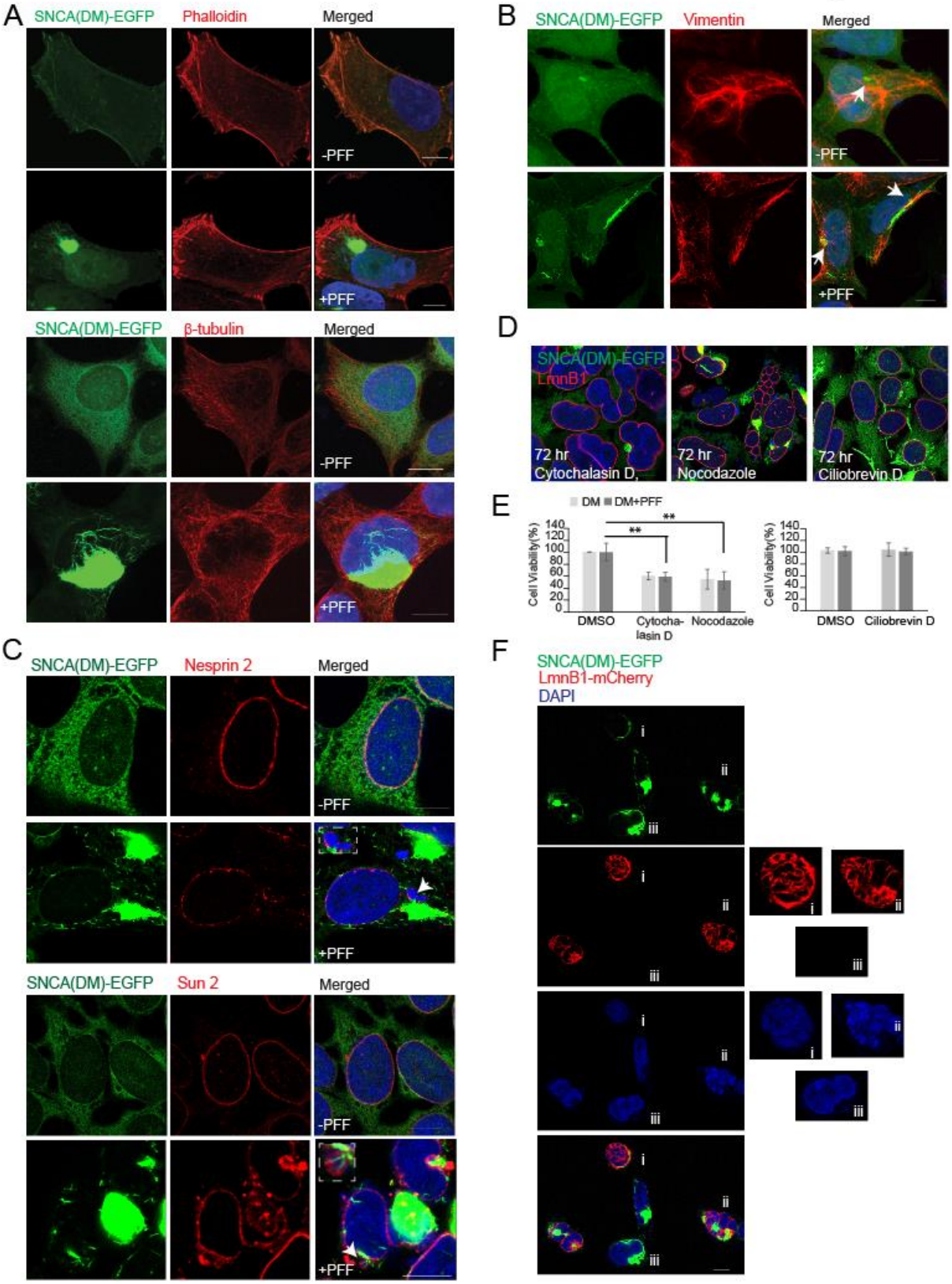
A
SNCA(DM)-EGFP
Phalloidin
Merged
-PFF
+PFF
SNCA(DM)-EGFP
β-tubulin
Merged
-PFF
+PFF
B
SNCA(DM)-EGFP
Vimentin
Merged
-PFF
+PFF
C
SNCA(DM)-EGFP
Nesprin 2
Merged
-PFF
+PFF
SNCA(DM)-EGFP
Sun 2
Merged
-PFF
+PFF
D
SNCA(DM)-EGFP
LmnB1
72 hr
Cytochalasin D
72 hr
Nocodazole
72 hr
Ciliobrevin D
E
DM
DM+PFF
Cell Viability(%)
DMSO
Cytocha-lasin D
Nocodazole
Ciliobrevin D
F
SNCA(DM)-EGFP
LmnB1-mCherry
DAPI

Fig. S5: Cytoskeleton, Nucleoskeleton, Perinuclear Syn-filaments and Nuclear injuries.

A-C: Microscopic images shown in **Fig. 5A, 5B and 5C** – images of fluorescent proteins/antibodies excited by different wavelengths of lasers are shown separately.

D: Morphology of 6th day SNCA(DM)-EGFP cells immunostained with LmnB1. Cells were treated as indicated in figure.

E: SNCA(DM)-EGFP +/- PFF cells were treated with Nocodazole, Cytochalasin D and Ciliobrevin D on 3rd day of PFF incubation, incubated further for 3 days and MTT assay was performed. N = 4. ** = p-value <0.005, Student's *t*-test.

F: Microscopic images shown in **Fig. 5J** – images of fluorescent proteins/antibodies excited by different wavelengths of lasers are shown separately. Zoomed images of sites **i**, **ii** and **iii** are shown on the Right.

Scale bar – 10 μm.

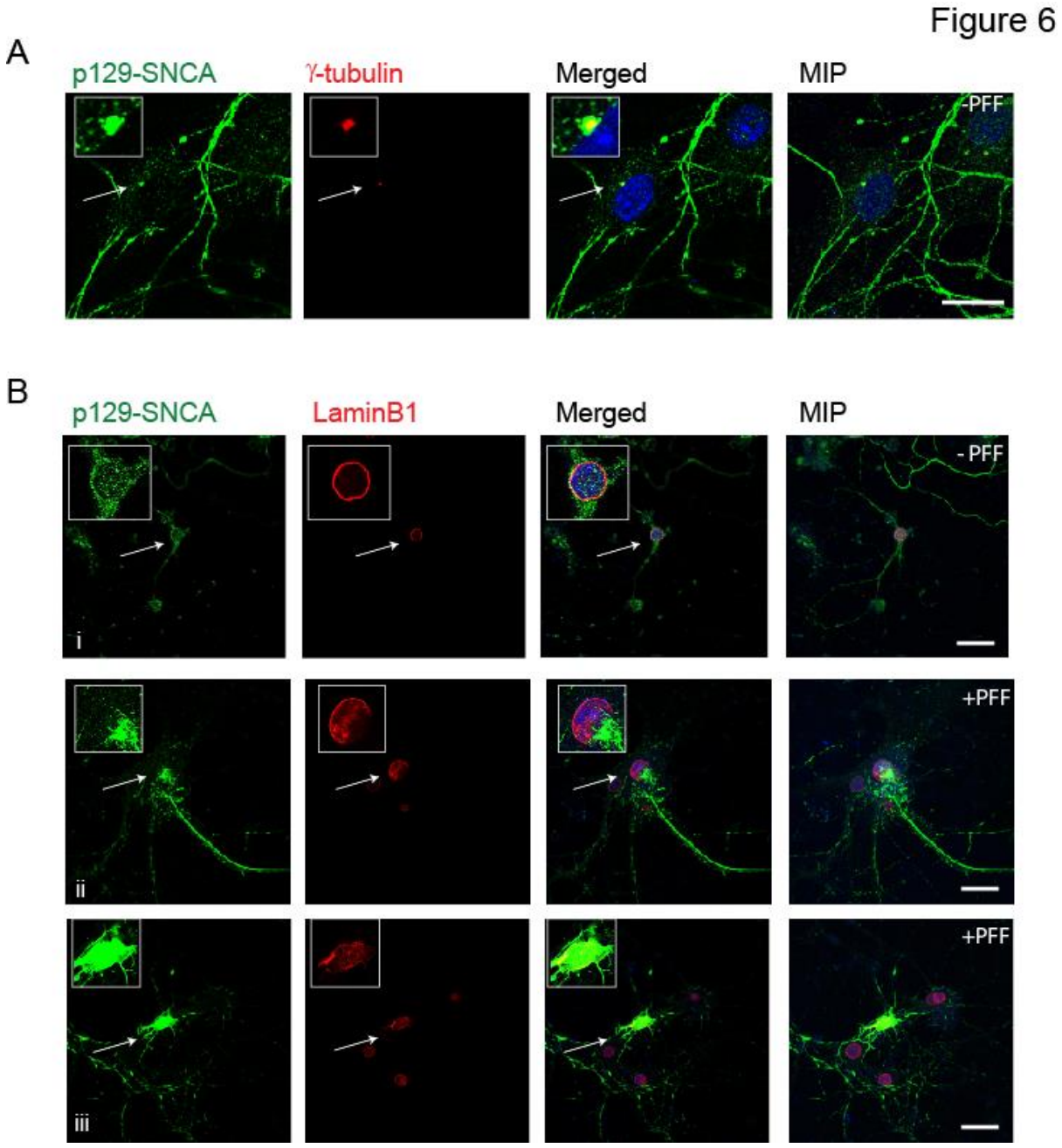

Fig 6. Syn-aggresomes, Syn-filaments, and nuclear injuries in primary neurons

A: Primary neurons at 15 days *in vitro* (DIV) were fixed and immunostained with p129-Syn and γ-tubulin antibody.

B: Primary neurons at 15 DIV without PFF treatment (**i**) and 10 days post PFF treatment (**ii** and **iii**) were fixed and immunostained with p129-Syn and LmnB1.

Insets: zoomed images of the arrow indicated locations. Scale bar- 20 µm.

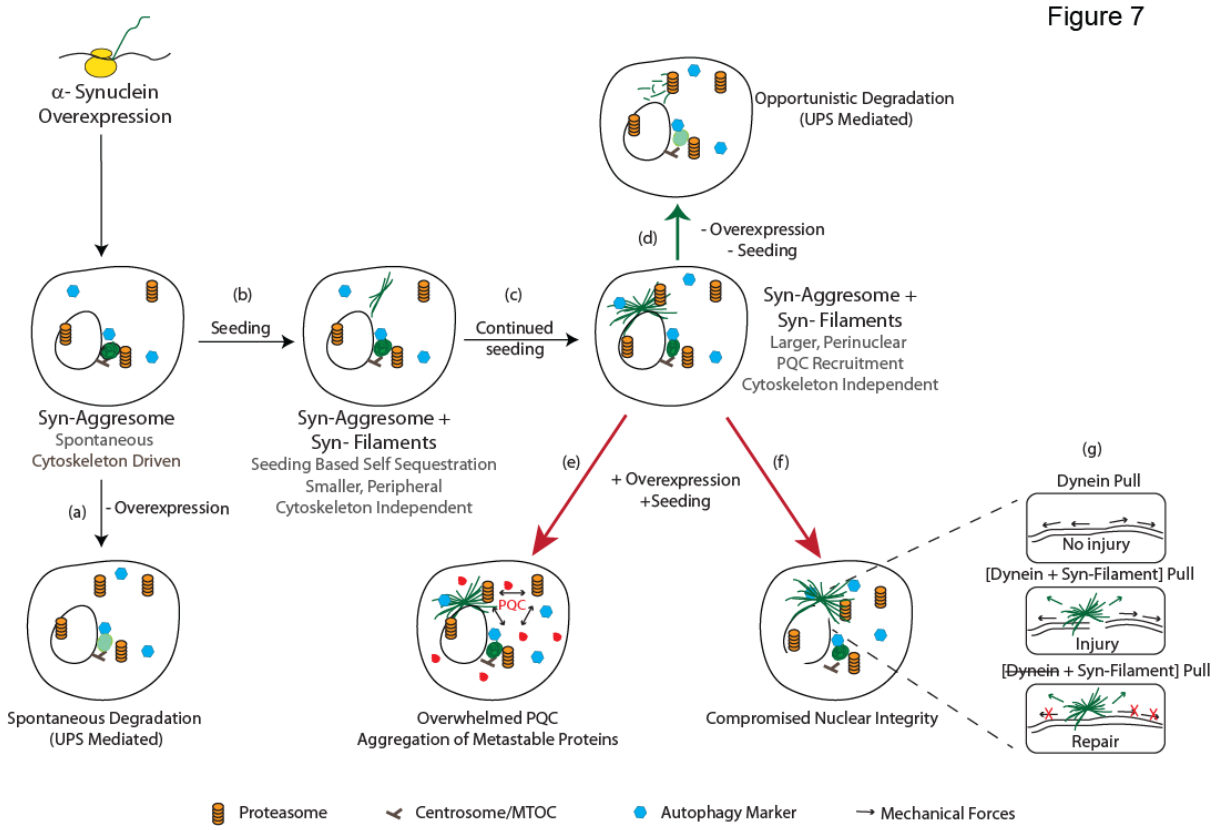

Fig. 7: Model depicting two distinct α-Synuclein inclusion bodies in the same cell offering unique homeostatic consequences: **(a)** Syn-aggresomes are formed spontaneously upon overexpression of α-Synuclein and assist UPS mediated degradation of the overexpressed protein. **(b)** Syn-filaments are induced by the addition of seeds in the same cells and are not recognized by PQC factors at early stage. **(c)** PQC components are recruited to over-grown perinuclear Syn-filaments. **(d)** Syn-filaments remain UPS-degradable upon withdrawal of seeds or after stopping α-Synuclein expression. **(e)** In case of continued polymerization, repurposing of PQC-factors to large Syn-filaments oversaturates proteostasis resulting in aggregation of other misfolding-prone proteins; in the current example FlucDM-mCherry (red). **(f-g)** Large Syn-filaments associate with nuclear envelope to weaken the lamina and dynein motor forces pull apart the nuclear lamina, resulting in extensive nuclear injury.

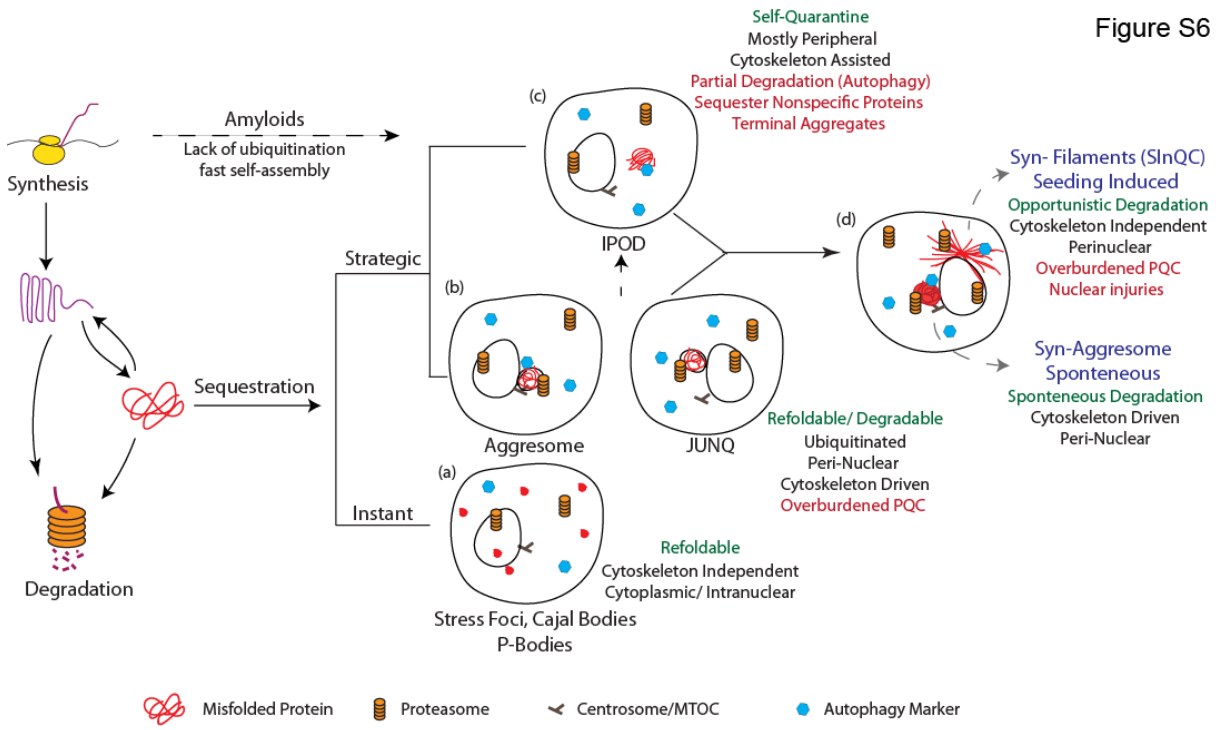

Fig. S6: Different strategies to sequester misfolded protein load in the cell. (a) Misfolding-prone proteins are sequestered into multiple reversible stress foci in cytoplasm and nucleus instantaneously after acute stress such as heat shock. (**b**) Upon continuous stress, misfolding prone proteins are ubiquitinated and directed to perinuclear sites in cytoskeleton driven manner. These are called aggresomes or JUNQs depending on their position on MTOC or their proximity to perinuclear endoplasmic reticulum. Both aggresomes and JUNQs serve as sites for refolding or degradation of misfolded proteins depending on their recognition by PQC-factors. **(c)** Upon saturation of the capacity of aggresomes/JUNQs, further increased load of misfolded proteins are sequestered into peripheral sites known as IPODs. Proteins accumulated into IPODs are terminally aggregated and avoid non-specific interactions with cellular proteins. IPODs are occasionally degraded by autophagy machinery or diluted through division in mitotic cells. Amyloids possessing faster self-polymerization properties are proposed to directly accumulate into IPODs bypassing aggresomes/JUNQs. **(d)** Misfolding prone α-Synuclein spontaneously accumulate into **Syn-aggresomes** for continuous turnover and into **Syn-filaments** upon seeding. Syn-filaments remain

opportunistically UPS-degradable like aggresomes. Syn-filaments also share the self-sequestration properties of IPODs, remain less interactive and seclude misfolding prone α-Synuclein from the rest of the proteome. Thus, Syn-filaments represent a unique homeostatic inclusion body sharing properties of both aggresomes and IPODs and we term these as **SInQCs – Seeding based Inclusions for Quality Control**.

References

Agrawal A, Lele TP (2019) Mechanics of nuclear membranes. *J Cell Sci* 132

Ahmad MF, Ramakrishna T, Raman B, Rao Ch M (2006) Fibrillogenic and non-fibrillogenic ensembles of SDS-bound human alpha-synuclein. *J Mol Biol* 364: 1061-72

Bauerlein FJB, Fernandez-Busnadiego R, Baumeister W (2020) Investigating the Structure of Neurotoxic Protein Aggregates Inside Cells. *Trends Cell Biol* 30: 951-966

Beaudouin J, Gerlich D, Daigle N, Eils R, Ellenberg J (2002) Nuclear envelope breakdown proceeds by microtubule-induced tearing of the lamina. *Cell* 108: 83-96

Buratti E, Baralle FE (2012) TDP-43: gumming up neurons through protein-protein and protein-RNA interactions. *Trends Biochem Sci* 37: 237-47

Burke B, Stewart CL (2013) The nuclear lamins: flexibility in function. *Nat Rev Mol Cell Biol* 14: 13-24

Burre J, Sharma M, Sudhof TC (2018) Cell Biology and Pathophysiology of alpha-Synuclein. *Cold Spring Harb Perspect Med* 8

Chen B, Retzlaff M, Roos T, Frydman J (2011) Cellular strategies of protein quality control. *Cold Spring Harb Perspect Biol* 3: a004374

Chen V, Moncalvo M, Tringali D, Tagliafierro L, Shriskanda A, Ilich E, Dong W, Kantor B, Chiba-Falek O (2020) The mechanistic role of alpha-synuclein in the nucleus: impaired nuclear function caused by familial Parkinson's disease SNCA mutations. *Hum Mol Genet* 29: 3107-3121

Conway KA, Lee SJ, Rochet JC, Ding TT, Harper JD, Williamson RE, Lansbury PT, Jr. (2000a) Accelerated oligomerization by Parkinson's disease linked alpha-synuclein mutants. *Ann N Y Acad Sci* 920: 42-5

Conway KA, Lee SJ, Rochet JC, Ding TT, Williamson RE, Lansbury PT, Jr. (2000b) Acceleration of oligomerization, not fibrillization, is a shared property of both alpha-synuclein mutations linked to early-onset Parkinson's disease: implications for pathogenesis and therapy. *Proc Natl Acad Sci U S A* 97: 571-6

Cox J, Mann M (2008) MaxQuant enables high peptide identification rates, individualized p.p.b.-range mass accuracies and proteome-wide protein quantification. *Nat Biotechnol* 26: 1367-72

Crisp M, Liu Q, Roux K, Rattner JB, Shanahan C, Burke B, Stahl PD, Hodzic D (2006) Coupling of the nucleus and cytoplasm: role of the LINC complex. *J Cell Biol* 172: 41-53

Culver BP, Savas JN, Park SK, Choi JH, Zheng S, Zeitlin SO, Yates JR, 3rd, Tanese N (2012) Proteomic analysis of wild-type and mutant huntingtin associated proteins in mouse brains identifies unique interactions and involvement in protein synthesis. *J Biol Chem*

Curran S, Wrigley M (1997) Lewy bodies. *Am J Psychiatry* 154: 1322-3

Davidson PM, Cadot B (2021) Actin on and around the Nucleus. *Trends Cell Biol* 31: 211-223

de Leeuw R, Gruenbaum Y, Medalia O (2018) Nuclear Lamins: Thin Filaments with Major Functions. *Trends Cell Biol* 28: 34-45

De Vos WH, Houben F, Kamps M, Malhas A, Verheyen F, Cox J, Manders EM, Verstraeten VL, van Steensel MA, Marcelis CL, van den Wijngaard A, Vaux DJ, Ramaekers FC, Broers JL (2011) Repetitive

disruptions of the nuclear envelope invoke temporary loss of cellular compartmentalization in laminopathies. *Hum Mol Genet* 20: 4175-86
Dey G, Baum B (2021) Nuclear envelope remodelling during mitosis. *Curr Opin Cell Biol* 70: 67-74
Economo MN, Viswanathan S, Tasic B, Bas E, Winnubst J, Menon V, Graybuck LT, Nguyen TN, Smith KA, Yao Z, Wang L, Gerfen CR, Chandrashekar J, Zeng H, Looger LL, Svoboda K (2018) Distinct descending motor cortex pathways and their roles in movement. *Nature* 563: 79-84
Engelender S, Kaminsky Z, Guo X, Sharp AH, Amaravi RK, Kleiderlein JJ, Margolis RL, Troncoso JC, Lanahan AA, Worley PF, Dawson VL, Dawson TM, Ross CA (1999) Synphilin-1 associates with alpha-synuclein and promotes the formation of cytosolic inclusions. *Nat Genet* 22: 110-4
Ferrera D, Canale C, Marotta R, Mazzaro N, Gritti M, Mazzanti M, Capellari S, Cortelli P, Gasparini L (2014) Lamin B1 overexpression increases nuclear rigidity in autosomal dominant leukodystrophy fibroblasts. *FASEB J* 28: 3906-18
Forno LS (1996) Neuropathology of Parkinson's disease. *J Neuropathol Exp Neurol* 55: 259-72
Galloway PG, Mulvihill P, Perry G (1992) Filaments of Lewy bodies contain insoluble cytoskeletal elements. *Am J Pathol* 140: 809-22
Gasset-Rosa F, Chillon-Marinas C, Goginashvili A, Atwal RS, Artates JW, Tabet R, Wheeler VC, Bang AG, Cleveland DW, Lagier-Tourenne C (2017) Polyglutamine-Expanded Huntingtin Exacerbates Age-Related Disruption of Nuclear Integrity and Nucleocytoplasmic Transport. *Neuron* 94: 48-57 e4
Guo Y, Zheng Y (2015) Lamins position the nuclear pores and centrosomes by modulating dynein. *Mol Biol Cell* 26: 3379-89
Gupta A, Sharif K, Walters M, Woods MD, Potty A, Main BJ, El-Amin SF, 3rd Surgical retrieval, isolation and in vitro expansion of human anterior cruciate ligament-derived cells for tissue engineering applications. *J Vis Exp*
Gupta R, Kasturi P, Bracher A, Loew C, Zheng M, Villella A, Garza D, Hartl FU, Raychaudhuri S (2011) Firefly luciferase mutants as sensors of proteome stress. *Nat Methods* 8: 879-884
Hardenberg MC, Sinnige T, Casford S, Dada S, Poudel C, Robinson EA, Fuxreiter M, Kaminksi C, Kaminski-Schierle GS, Nollen EAA, Dobson CM, Vendruscolo M (2021) Observation of an alpha-synuclein liquid droplet state and its maturation into Lewy body-like assemblies. *J Mol Cell Biol*
Hatch EM (2018) Nuclear envelope rupture: little holes, big openings. *Curr Opin Cell Biol* 52: 66-72
Hatch EM, Hetzer MW (2016) Nuclear envelope rupture is induced by actin-based nucleus confinement. *J Cell Biol* 215: 27-36
Henderson MX, Chung CH, Riddle DM, Zhang B, Gathagan RJ, Seeholzer SH, Trojanowski JQ, Lee VMY (2017) Unbiased Proteomics of Early Lewy Body Formation Model Implicates Active Microtubule Affinity-Regulating Kinases (MARKs) in Synucleinopathies. *J Neurosci* 37: 5870-5884
Herzig RP, Andersson U, Scarpulla RC (2000) Dynein light chain interacts with NRF-1 and EWG, structurally and functionally related transcription factors from humans and drosophila. *J Cell Sci* 113 Pt 23: 4263-73
Houben F, Ramaekers FC, Snoeckx LH, Broers JL (2007) Role of nuclear lamina-cytoskeleton interactions in the maintenance of cellular strength. *Biochim Biophys Acta* 1773: 675-86
Houthaeve G, Robijns J, Braeckmans K, De Vos WH (2018) Bypassing Border Control: Nuclear Envelope Rupture in Disease. *Physiology (Bethesda)* 33: 39-49
Johnston JA, Ward CL, Kopito RR (1998) Aggresomes: a cellular response to misfolded proteins. *J Cell Biol* 143: 1883-98
Kaganovich D, Kopito R, Frydman J (2008) Misfolded proteins partition between two distinct quality control compartments. *Nature* 454: 1088-95
Kapitein LC, Hoogenraad CC (2015) Building the Neuronal Microtubule Cytoskeleton. *Neuron* 87: 492-506
Karoutas A, Akhtar A (2021) Functional mechanisms and abnormalities of the nuclear lamina. *Nat Cell Biol* 23: 116-126

Kilpelainen T, Julku UH, Svarcbahs R, Myohanen TT (2019) Behavioural and dopaminergic changes in double mutated human A30P*A53T alpha-synuclein transgenic mouse model of Parkinson s disease. *Sci Rep* 9: 17382
Kim YE, Hosp F, Frottin F, Ge H, Mann M, Hayer-Hartl M, Hartl FU (2016) Soluble Oligomers of PolyQ-Expanded Huntingtin Target a Multiplicity of Key Cellular Factors. *Mol Cell* 63: 951-64
Kontopoulos E, Parvin JD, Feany MB (2006) Alpha-synuclein acts in the nucleus to inhibit histone acetylation and promote neurotoxicity. *Hum Mol Genet* 15: 3012-23
Kumar R, Nawroth PP, Tyedmers J (2016) Prion Aggregates Are Recruited to the Insoluble Protein Deposit (IPOD) via Myosin 2-Based Vesicular Transport. *PLoS Genet* 12: e1006324
Lammerding J, Wolf K (2016) Nuclear envelope rupture: Actin fibers are putting the squeeze on the nucleus. *J Cell Biol* 215: 5-8
Lashuel HA (2020) Do Lewy bodies contain alpha-synuclein fibrils? and Does it matter? A brief history and critical analysis of recent reports. *Neurobiol Dis* 141: 104876
Lazaro DF, Rodrigues EF, Langohr R, Shahpasandzadeh H, Ribeiro T, Guerreiro P, Gerhardt E, Krohnert K, Klucken J, Pereira MD, Popova B, Kruse N, Mollenhauer B, Rizzoli SO, Braus GH, Danzer KM, Outeiro TF (2014) Systematic comparison of the effects of alpha-synuclein mutations on its oligomerization and aggregation. *PLoS Genet* 10: e1004741
Lee HJ, Shin SY, Choi C, Lee YH, Lee SJ (2002) Formation and removal of alpha-synuclein aggregates in cells exposed to mitochondrial inhibitors. *J Biol Chem* 277: 5411-7
Lendel C, Bertoncini CW, Cremades N, Waudby CA, Vendruscolo M, Dobson CM, Schenk D, Christodoulou J, Toth G (2009) On the mechanism of nonspecific inhibitors of protein aggregation: dissecting the interactions of alpha-synuclein with Congo red and lacmoid. *Biochemistry* 48: 8322-34
Liu KY, Shyu YC, Barbaro BA, Lin YT, Chern Y, Thompson LM, James Shen CK, Marsh JL (2015) Disruption of the nuclear membrane by perinuclear inclusions of mutant huntingtin causes cell-cycle re-entry and striatal cell death in mouse and cell models of Huntington's disease. *Hum Mol Genet* 24: 1602-16
Liu X, Lee YJ, Liou LC, Ren Q, Zhang Z, Wang S, Witt SN (2011) Alpha-synuclein functions in the nucleus to protect against hydroxyurea-induced replication stress in yeast. *Hum Mol Genet* 20: 3401-14
Luk KC, Song C, O'Brien P, Stieber A, Branch JR, Brunden KR, Trojanowski JQ, Lee VM (2009) Exogenous alpha-synuclein fibrils seed the formation of Lewy body-like intracellular inclusions in cultured cells. *Proc Natl Acad Sci U S A* 106: 20051-6
Mahul-Mellier AL, Burtscher J, Maharjan N, Weerens L, Croisier M, Kuttler F, Leleu M, Knott GW, Lashuel HA (2020) The process of Lewy body formation, rather than simply alpha-synuclein fibrillization, is one of the major drivers of neurodegeneration. *Proc Natl Acad Sci U S A* 117: 4971-4982
Maroteaux L, Campanelli JT, Scheller RH (1988) Synuclein: a neuron-specific protein localized to the nucleus and presynaptic nerve terminal. *J Neurosci* 8: 2804-15
McFarland MA, Ellis CE, Markey SP, Nussbaum RL (2008) Proteomics analysis identifies phosphorylation-dependent alpha-synuclein protein interactions. *Mol Cell Proteomics* 7: 2123-37
McLean PJ, Kawamata H, Hyman BT (2001) Alpha-synuclein-enhanced green fluorescent protein fusion proteins form proteasome sensitive inclusions in primary neurons. *Neuroscience* 104: 901-12
McMurray CT (2000) Neurodegeneration: diseases of the cytoskeleton? *Cell Death Differ* 7: 861-5
McNaught KS, Shashidharan P, Perl DP, Jenner P, Olanow CW (2002) Aggresome-related biogenesis of Lewy bodies. *Eur J Neurosci* 16: 2136-48
Mikenberg I, Widera D, Kaus A, Kaltschmidt B, Kaltschmidt C (2007) Transcription factor NF-kappaB is transported to the nucleus via cytoplasmic dynein/dynactin motor complex in hippocampal neurons. *PLoS One* 2: e589
Nonaka T, Hasegawa M (2009) A cellular model to monitor proteasome dysfunction by alpha-synuclein. *Biochemistry* 48: 8014-22

Ogrodnik M, Salmonowicz H, Brown R, Turkowska J, Sredniawa W, Pattabiraman S, Amen T, Abraham AC, Eichler N, Lyakhovetsky R, Kaganovich D (2014) Dynamic JUNQ inclusion bodies are asymmetrically inherited in mammalian cell lines through the asymmetric partitioning of vimentin. *Proc Natl Acad Sci U S A* 111: 8049-54
Olanow CW, Perl DP, DeMartino GN, McNaught KS (2004) Lewy-body formation is an aggresome-related process: a hypothesis. *Lancet Neurol* 3: 496-503
Olzscha H, Schermann SM, Woerner AC, Pinkert S, Hecht MH, Tartaglia GG, Vendruscolo M, Hayer-Hartl M, Hartl FU, Vabulas RM (2011) Amyloid-like aggregates sequester numerous metastable proteins with essential cellular functions. *Cell* 144: 67-78
Park SH, Kukushkin Y, Gupta R, Chen T, Konagai A, Hipp MS, Hayer-Hartl M, Hartl FU (2013) PolyQ Proteins Interfere with Nuclear Degradation of Cytosolic Proteins by Sequestering the Sis1p Chaperone. *Cell* 154: 134-45
Penfield L, Wysolmerski B, Mauro M, Farhadifar R, Martinez MA, Biggs R, Wu HY, Broberg C, Needleman D, Bahmanyar S (2018) Dynein pulling forces counteract lamin-mediated nuclear stability during nuclear envelope repair. *Mol Biol Cell* 29: 852-868
Pinho R, Paiva I, Jercic KG, Fonseca-Ornelas L, Gerhardt E, Fahlbusch C, Garcia-Esparcia P, Kerimoglu C, Pavlou MAS, Villar-Pique A, Szego E, Lopes da Fonseca T, Odoardi F, Soeroes S, Rego AC, Fischle W, Schwamborn JC, Meyer T, Kugler S, Ferrer I et al. (2019) Nuclear localization and phosphorylation modulate pathological effects of alpha-synuclein. *Hum Mol Genet* 28: 31-50
Ramdzan YM, Trubetskov MM, Ormsby AR, Newcombe EA, Sui X, Tobin MJ, Bongiovanni MN, Gras SL, Dewson G, Miller JML, Finkbeiner S, Moily NS, Niclis J, Parish CL, Purcell AW, Baker MJ, Wilce JA, Waris S, Stojanovski D, Bocking T et al. (2017) Huntingtin Inclusions Trigger Cellular Quiescence, Deactivate Apoptosis, and Lead to Delayed Necrosis. *Cell Rep* 19: 919-927
Rappsilber J, Ishihama Y, Mann M (2003) Stop and go extraction tips for matrix-assisted laser desorption/ionization, nanoelectrospray, and LC/MS sample pretreatment in proteomics. *Anal Chem* 75: 663-70
Rawat S, Anusha V, Jha M, Sreedurgalakshmi K, Raychaudhuri S (2019) Aggregation of Respiratory Complex Subunits Marks the Onset of Proteotoxicity in Proteasome Inhibited Cells. *J Mol Biol* 431: 996-1015
Ray S, Singh N, Kumar R, Patel K, Pandey S, Datta D, Mahato J, Panigrahi R, Navalkar A, Mehra S, Gadhe L, Chatterjee D, Sawner AS, Maiti S, Bhatia S, Gerez JA, Chowdhury A, Kumar A, Padinhateeri R, Riek R et al. (2020) alpha-Synuclein aggregation nucleates through liquid-liquid phase separation. *Nat Chem* 12: 705-716
Richfield EK, Thiruchelvam MJ, Cory-Slechta DA, Wuertzer C, Gainetdinov RR, Caron MG, Di Monte DA, Federoff HJ (2002) Behavioral and neurochemical effects of wild-type and mutated human alpha-synuclein in transgenic mice. *Exp Neurol* 175: 35-48
Salina D, Bodoor K, Eckley DM, Schroer TA, Rattner JB, Burke B (2002) Cytoplasmic dynein as a facilitator of nuclear envelope breakdown. *Cell* 108: 97-107
Sanchez I, Mahlke C, Yuan J (2003) Pivotal role of oligomerization in expanded polyglutamine neurodegenerative disorders. *Nature* 421: 373-9
Seibenhener ML, Wooten MW (2012) Isolation and culture of hippocampal neurons from prenatal mice. *J Vis Exp*
Shevchenko A, Wilm M, Vorm O, Mann M (1996) Mass spectrometric sequencing of proteins silver-stained polyacrylamide gels. *Anal Chem* 68: 850-8
Smoyer CJ, Jaspersen SL (2014) Breaking down the wall: the nuclear envelope during mitosis. *Curr Opin Cell Biol* 26: 1-9
Song J, Yang Q, Yang J, Larsson L, Hao X, Zhu X, Malmgren-Hill S, Cvijovic M, Fernandez-Rodriguez J, Grantham J, Gustafsson CM, Liu B, Nystrom T (2014) Essential genetic interactors of SIR2 required for spatial sequestration and asymmetrical inheritance of protein aggregates. *PLoS Genet* 10: e1004539

Sontag EM, Vonk WIM, Frydman J (2014) Sorting out the trash: the spatial nature of eukaryotic protein quality control. *Curr Opin Cell Biol* 26: 139-146
Spillantini MG, Crowther RA, Jakes R, Hasegawa M, Goedert M (1998) alpha-Synuclein in filamentous inclusions of Lewy bodies from Parkinson's disease and dementia with lewy bodies. *Proc Natl Acad Sci U S A* 95: 6469-73
Spokoini R, Moldavski O, Nahmias Y, England JL, Schuldiner M, Kaganovich D (2012) Confinement to organelle-associated inclusion structures mediates asymmetric inheritance of aggregated protein in budding yeast. *Cell Rep* 2: 738-47
Taylor JP, Tanaka F, Robitschek J, Sandoval CM, Taye A, Markovic-Plese S, Fischbeck KH (2003) Aggresomes protect cells by enhancing the degradation of toxic polyglutamine-containing protein. *Hum Mol Genet* 12: 749-57
Treusch S, Cyr DM, Lindquist S (2009) Amyloid deposits: protection against toxic protein species? *Cell Cycle* 8: 1668-74
Tyanova S, Temu T, Sinitcyn P, Carlson A, Hein MY, Geiger T, Mann M, Cox J (2016) The Perseus computational platform for comprehensive analysis of (prote)omics data. *Nat Methods* 13: 731-40
Tyedmers J, Mogk A, Bukau B (2010a) Cellular strategies for controlling protein aggregation. *Nat Rev Mol Cell Biol* 11: 777-88
Tyedmers J, Treusch S, Dong J, McCaffery JM, Bevis B, Lindquist S (2010b) Prion induction involves an ancient system for the sequestration of aggregated proteins and heritable changes in prion fragmentation. *Proc Natl Acad Sci U S A* 107: 8633-8
Vizcaino JA, Deutsch EW, Wang R, Csordas A, Reisinger F, Rios D, Dianes JA, Sun Z, Farrah T, Bandeira N, Binz PA, Xenarios I, Eisenacher M, Mayer G, Gatto L, Campos A, Chalkley RJ, Kraus HJ, Albar JP, Martinez-Bartolome S et al. (2014) ProteomeXchange provides globally coordinated proteomics data submission and dissemination. *Nat Biotechnol* 32: 223-6
Volpicelli-Daley LA, Luk KC, Lee VM (2014) Addition of exogenous alpha-synuclein preformed fibrils to primary neuronal cultures to seed recruitment of endogenous alpha-synuclein to Lewy body and Lewy neurite-like aggregates. *Nat Protoc* 9: 2135-46
Volpicelli-Daley LA, Luk KC, Patel TP, Tanik SA, Riddle DM, Stieber A, Meaney DF, Trojanowski JQ, Lee VM (2011) Exogenous alpha-synuclein fibrils induce Lewy body pathology leading to synaptic dysfunction and neuron death. *Neuron* 72: 57-71
Waelter S, Boeddrich A, Lurz R, Scherzinger E, Lueder G, Lehrach H, Wanker EE (2001) Accumulation of mutant huntingtin fragments in aggresome-like inclusion bodies as a result of insufficient protein degradation. *Mol Biol Cell* 12: 1393-407
Weisberg SJ, Lyakhovetsky R, Werdiger AC, Gitler AD, Soen Y, Kaganovich D (2012) Compartmentalization of superoxide dismutase 1 (SOD1G93A) aggregates determines their toxicity. *Proc Natl Acad Sci U S A* 109: 15811-6